

# TRG-Net: An Interpretable and Controllable Rain Generator

Zhiqiang Pang, Hong Wang, Qi Xie, Deyu Meng, Zongben Xu

School of Mathematics and Statistics, Xi'an Jiaotong University, Xi'an, Shaanxi, China.

Contributing authors: [xjtupzq@gmail.com](mailto:xjtupzq@gmail.com); [hongwang9209@hotmail.com](mailto:hongwang9209@hotmail.com);  
[xie.qi@mail.xjtu.edu.cn](mailto:xie.qi@mail.xjtu.edu.cn); [dymeng@mail.xjtu.edu.cn](mailto:dymeng@mail.xjtu.edu.cn); [zbxu@mail.xjtu.edu.cn](mailto:zbxu@mail.xjtu.edu.cn);

## Abstract

Exploring and modeling rain generation mechanism is critical for augmenting paired data to ease training of rainy image processing models. Against this task, this study proposes a novel deep learning based rain generator, which fully takes the physical generation mechanism underlying rains into consideration and well encodes the learning of the fundamental rain factors (i.e., shape, orientation, length, width and sparsity) explicitly into the deep network. Its significance lies in that the generator not only elaborately design essential elements of the rain to simulate expected rains, like conventional artificial strategies, but also finely adapt to complicated and diverse practical rainy images, like deep learning methods. By rationally adopting filter parameterization technique, we first time achieve a deep network that is finely controllable with respect to rain factors and able to learn the distribution of these factors purely from data. Our unpaired generation experiments demonstrate that the rain generated by the proposed rain generator is not only of higher quality, but also more effective for deraining and downstream tasks compared to current state-of-the-art rain generation methods. Besides, the paired data augmentation experiments, including both in-distribution and out-of-distribution (OOD), further validate the diversity of samples generated by our model for in-distribution deraining and OOD generalization tasks.

**Keywords:** Rain generation, Interpretable network, Unpaired data generation, Data augmentation

## 1 Introduction

Exploring and modeling rain generation mechanism is critical for augmenting paired data to ease the training of rainy image processing models. This is especially meaningful for current deep learning based image rain removal methods, where the effectiveness is highly dependent on paired rainy and rainless images [1–4]. However, ideal data pairs are always hard to collect, particularly in the complicated and diverse rain scenarios in practice. Besides, the rain generation task is also of great potential value in revealing insightful characteristics underlying real rains, helpful in

guiding sound policies for dealing with practical severe weather emergencies [5–7].

The early methods for investigating how to generate rainy images are mainly physical rendering based artificial synthesis manners [8–10]. Specifically, as shown in Fig. 1, there are mainly three parts for generating a rainy image. The first part is the rain kernel model, for generating convolution kernels that involve the orientation, length, width and other shape information of the rain streaks. The second part is the rain map model, which is decided by the sparsity and position of the rains. By convolving the rain kernel and rain map, we can obtain a lifelike rain streak image. The final part is a merging model that simulates

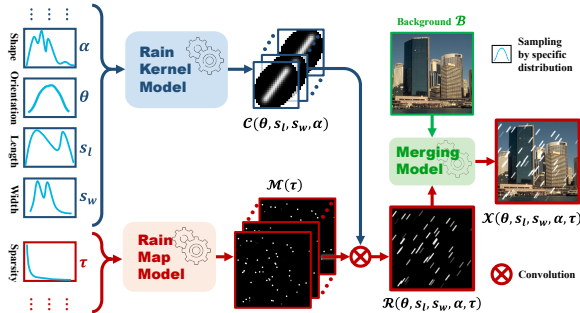


**Fig. 1** The pipeline for artificial rainy image synthesis based on physical rendering. It mainly contains three parts: (a) rain kernel model, (b) rain map model, and (c) merging model.

the interaction between rain streaks and a background image (e.g., rain streak photometry and fog-like rain). By carefully designing the three generation parts, rainy images can be synthesized with controllable shape, orientation, width, length and sparsity, even without any model training process. This manner has been widely used in the generation of rain scenes in movies, video games, animations and artistic works [11, 12].

Although this category of methods can synthesize visually lifelike rainy images in the sense of human intuition, it still lacks realism to use the synthesized rainy/rainless images to train deep neural networks for deraining [13, 14]. This is because the generation models of these methods are designed purely by human subjectivity, which inevitably leads to differences with the more complicated and diverse rains in real scenes.

Very recently, deep learning (DL) based manners have been exploited for this task. The basic idea is to adopt generative adversarial networks (GANs) to train a rain generator and a discriminator, where the generator captures the rainy data distribution, and the discriminator distinguishes the difference between the real rains and the generated ones [15–17]. In this way, the generated rains are forced to get close to the real rains in terms of the probability distribution through the training with real samples. It has been shown that the rainy/rainless image pairs generated in this way can help to achieve a great performance improvement in deraining tasks [18–20].

However, the current rain synthesis methods based on GANs still have obvious drawbacks. The most critical one is the design of rain generators. In particular, the current rain generators

are usually assembled with some off-the-shelf network modules in commonly-adopted deep learning toolkits, e.g., convolutional neural networks (CNNs), which is indeed a “black box” without considering the intrinsic rain generation mechanism, and thus increases the learning difficulty and data requirements. Moreover, this insufficient knowledge modeling issue makes these methods hardly be effectively trained under the condition of inadequate paired training data, like those with unpaired rainy/rainless images [18–22]. A more popular way is to use these GAN-based generators just for data augmentation from a small number of paired data samples [18, 19]. However, the problem of paired data collection still remains in this manner. It is thus critical to develop a rain generator capable of more faithfully delivering real rain generation mechanism for rain generation, with higher generation capability and lower data requirements.

Fortunately, the generation mechanism of rain streaks has been well studied in the previous physical rendering based artificial synthesis methods, where one can find that rain streaks are mainly decided by their shapes, orientations, widths, lengths and sparsity [8, 9, 23], as shown in Fig. 1. In this paper, we focus on intrinsically combining the advantages of the physical rendering based artificial synthesis methodology and the deep learning based one to design a dedicated generator for rain generation.

Specifically, we aim to design a deep learning based rain generator which is controllable with respect to the rain factors (i.e., shape, orientation, width, length of the rain kernel and sparsity of the rain map) just like conventional artificial synthesis methods, while the distribution of these rain factors can be learned through the generative adversarial manner instead of being manually preset. This is actually not that trivial to achieve, since the current CNNs cannot be easily controlled by the aforementioned rain factors. For example, for controlling the orientation of rain streak generation, we have to dynamically rotate an entire CNN architecture in its spatial dimensions, which is not easy to implement with common CNN architecture. It is even more difficult to learn the orientation distribution of the rain streak in the whole rainy image dataset. In this paper, we exploit the filter parametrization technique and

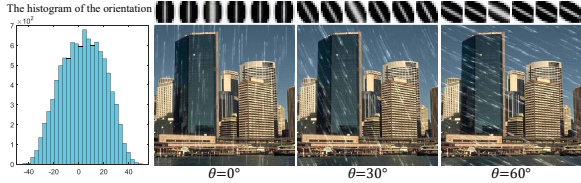


**Fig. 2** The orientation distribution (left figure) extracted from Rain100L by the proposed TRG-Net, which enables to generate rains with required orientation by specifying the orientation degree  $\theta$ . Here, we generate the rains with orientations of  $0^\circ$ ,  $30^\circ$  and  $60^\circ$ , respectively.

firstly design such an expected rain factor transformable convolution network for rain generation, where the aforementioned goals can all be finely achieved. Specifically, the main contributions of this paper are summarized as follows:

- We construct a new rain generator, which can properly extract fundamental rain factors underlying rainy images, including shape, orientation, width, length and sparsity, directly from data in a purely automatic manner. Its significance lies in that the model can both elaborately design fundamental elements to simulate expected rains like conventional artificial rendering manners, and finely adapt to complicated and diverse practical rain forms like recent deep learning methods. To the best of our knowledge, this should be the first method that is not only controllable with respect to rain factors, but also can learn the distribution of these factors purely from data. (e.g., Fig. 2 shows the extracted distribution about the orientation factor from Rain100L, finely complying with its real situation). The model is thus with intrinsic interpretability and essential controllability.
- To alleviate the difficulty in embedding controllable and learnable rain factors into deep networks, we construct a transformable convolution framework. Specifically, we exploit the filter parametrization technique [24] for representing convolution filters to ameliorate the original discrete expression as continuous when constructing CNNs. This makes the expected transformation operators, such as rotation and scaling, able to be imposed on the convolution filters more easily and soundly, while keeping them learnable. Under such transformable convolutions, we can naturally construct a transformable rain kernel model (in Sec. 4.2.1) and

rotatable CNNs (in Secs. 4.2.2 and 4.2.3). Moreover, we present a new total variation (TV) regularizer, called rotatable TV regularizer (in Sec. 4.3), capable of adaptively adjusting the orientation for calculating variations and adopting higher penalty along the rain streak orientation. The aforementioned functions could be potentially applied to a wider range of tasks.

- Our experiments show that the proposed model can effectively extract intrinsic physical mechanism implicitly contained in rainy images. The obtained rain factors, like orientation, scale and sparsity, are highly consistent with those reflected in the data, which can in turn be utilized to generate more variations of similar rain types with wider range of rain factors.
- Comprehensive experiments in both unpaired rain generation and paired rain augmentation further substantiate the superiority of the proposed method beyond current state-of-the-art (SOTA) methods. Specifically, in the unpaired generation experiments, it is demonstrated that the rain generated by the proposed generator is not only of higher quality, but also more effective for deraining and downstream tasks (e.g., semantic segmentation), as compared with those generated by competing methods. In the data augmentation experiments, including both in-distribution and out-of-distribution scenarios, it is further validated that the proposed method outperforms competing methods.

The paper is organized as follows. Sec. 2 reviews necessary related works. Sec. 3 presents the transformable convolution framework employed in our method. Sec. 4 then proposes details of our proposed transformable rain generator. Sec. 5 demonstrates comprehensive experiments to substantiate the effectiveness of the proposed method. The paper is finally concluded with future work.

## 2 Related Work

### 2.1 Rain Synthesis Methods

The most straightforward way to collect rainy/rainless image pairs is to utilize rainy videos, where rainy images come from the video frames and rainless images are estimated from a sequence of video frames [25, 26]. While this

method is able to collect the rainy images in real scenes, the resulting rainless images often contain remnants of rain streaks or lost image details.

Physical rendering based artificial synthesis is a common method that synthesizes rainy/rainless image pairs. The appearance of rain was studied early based on a raindrop oscillation model by Garg and Nayar [8, 9]. The rain streaks are considered to be the motion blur of the raindrops and can be synthesized with controllable shape, orientation, width, length and sparsity, by carefully setting the parameters of the rain model. Many rain datasets are constructed using the photorealistic rendering technique<sup>1</sup>. In general, rain streaks are first synthesized with physical models [8, 9], and then the rain streaks are blended to rainless background images to get the paired rainy images. Some works assume that rain streaks are simply superimposed to the background images, such as Rain100L [7, 27] and Rain800 [28]. Some works, such as Rain100H [7], Cityscapes [29, 30] and Kitti [29, 30], try to explore a more complex merge relationship between rain layer and background image. These large-scale paired rain datasets offer the training set for deraining networks and can quantitatively measure the effectiveness of deraining models. However, the rain streaks synthesized by these methods often tend to deviate from the real rains with much more complicated and diverse configurations. Such deviation usually leads to a degradation of the performance of the deraining models when dealing with the real rainy images.

Recently, GANs [15, 16] are employed for the rain generation where the probability distribution of the generated rain is forced to get close to that of the real rain through the training of certain generation network, which has achieved great success. Typically, [29–31] generated rains using the manually-designed rain models, and GANs are only adopted for learning the wetness scene. [18–20] generated rains using a generator stacked from some existing network modules and ignored the intrinsic rain generation mechanism, which is indeed a “black box” network. These methods tend to increase the learning difficulty and data requirements due to the neglecting of rain generation mechanism. Moreover, this insufficient

knowledge modeling issue also makes these methods hardly able to be sufficiently trained on the condition of inadequate paired training data, like those with unpaired rainy/rainless images [18, 19].

Different from previous rain synthesis methods, our aim is to intrinsically combine the advantages of both physical based methods and deep learning based methods, and design a deep rain factor transformable rain generator with intrinsic interpretability and essential controllability.

## 2.2 Single Image Rain Removal

Since single image rain removal (SIRR) is highly related to the investigated rain generation task in this study, we also briefly review the research works along this research line. The SIRR task aims to reconstruct the rain-free image from an image degraded by rain streaks. Recently, DL-based methods are the mainstream in SIRR. A flurry of network architectures, from simple CNNs [6, 7] to complicated architectures [25, 32, 33] and transformer-based ones [34], have been designed to handle this task. Although promising performance have been achieved, most of them are fully supervised and trained on synthetic rain data. The performance of these supervised derainers tend to drop dramatically when dealing with real-world rains, because there is a domain gap between the current synthesized and real rainy images.

There are some works trying to tackle this issue in a semi-supervised [13, 14] or unsupervised way [22, 35], but their performance is usually limited due to the lack of effective supervision information. Therefore, it is critical to design a rain generator for faithfully simulating real rain data with essentially more complexity and flexibly constructing paired datasets.

## 3 Transformable Convolution Framework

Traditional convolution kernels are usually discrete, which can’t be arbitrarily and accurately rotated or scaled. It is then natural to exploit continuous representation of convolution kernels for easily constructing transformable convolution. To this end, we employ filter parametrization methods to construct the overall framework of the transformable convolution as is shown in Fig. 3.

---

<sup>1</sup><https://www.photoshopessentials.com/photo-effects/rain/>

Specifically, the filter parametrization approach [36] regards a discrete convolution kernel  $\phi \in \mathbb{R}^{p \times p}$  as the discretization of a 2D continuous function  $\tilde{\phi}$  on the  $[-(p-1)/2, (p-1)/2]^2$  area. A typical formulation for constructing  $\tilde{\phi}(x)$  is [37]:

$$\tilde{\phi}(x) = \sum_{n=1}^N w_n \varphi_n(x), \forall x \in \mathbb{R}^2, \quad (1)$$

where  $\{w_n\}_{n=1}^N$  is representation coefficients, and  $\varphi_n(x)$  denotes the  $n^{\text{th}}$  basis function.

The key issue here is the choice of the basis function set. Especially, for rain generation task which requires pixel-level accuracy, it is important to choose a basis function set so that any discrete filter can be accurately represented, i.e., for any  $\phi$ , there exists a set of  $w_n$  so that  $\tilde{\phi}(x_{ij}) = \phi_{ij}$ . Besides, another issue here is to avoid aliasing effect<sup>2</sup>, otherwise the convolution kernel can be very unstable when being transformed [24, 36, 37].

Fortunately, it has been shown that Fourier series expansion based filter parametrization (FSE-FP) method [24] can not only lead to zero representation error for any  $\tilde{\phi}$ , but also well release the aliasing effect, which finely meets the requirements of our task. Specifically, the basis function set proposed in FSE-FP method is

$$\Phi = \{\varphi_{kl}^c(x), \varphi_{kl}^s(x) | k, l = 0, 1, \dots, p-1\}, \quad (2)$$

where

$$\begin{aligned} \varphi_{kl}^c(x) &= \Lambda(x) \cos\left(\frac{2\pi}{p} \left[ k - \left\lfloor \frac{p}{2} \right\rfloor, l - \left\lfloor \frac{p}{2} \right\rfloor \right] \cdot x\right), \\ \varphi_{kl}^s(x) &= \Lambda(x) \sin\left(\frac{2\pi}{p} \left[ k - \left\lfloor \frac{p}{2} \right\rfloor, l - \left\lfloor \frac{p}{2} \right\rfloor \right] \cdot x\right), \end{aligned} \quad (3)$$

where  $\Lambda(x) \geq 0$  is a radial mask function<sup>3</sup>, which satisfies  $\Lambda(x) = 0$  if  $\|x\| \geq (p+1)/2$  and  $\lfloor \cdot \rfloor$  represents the floor operator.

**Transformable convolution kernel.** Based on the parametrization method of Eqs. (1) and (3), we can implement any transformations on the convolution kernel  $\tilde{\phi}(x)$  through the corresponding

<sup>2</sup>The aliasing effect here is caused by the insufficient sampling rate of discrete filter when the bases frequency is too high, resulting in an incorrect transformation result. For a detailed analysis of the aliasing effect please refer to [24].

<sup>3</sup>The circular mask acts to limit the angle of basis functions, making them easier to transform. Please refer to [24] for more details of  $\Lambda(x)$ .

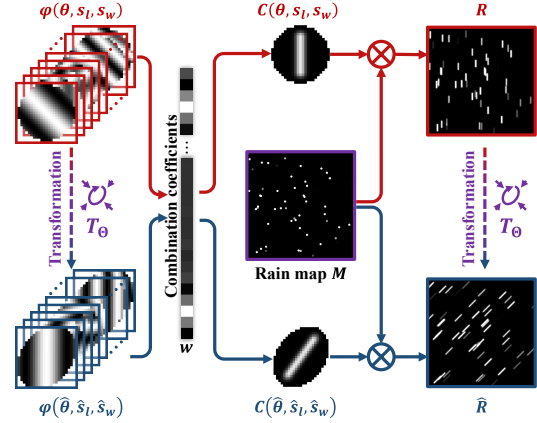


**Fig. 3** Transform the convolution output by the transformation of the convolution filter, which is achieved by functional transforms on the underlying 2D basis functions.  $\varphi(\theta, s_l, s_w)$  and  $\varphi(\hat{\theta}, \hat{s}_l, \hat{s}_w)$  are the basis function set (defined in Eqs. (2) and (3)) with different transformation parameters.  $C(\theta, s_l, s_w)$  and  $C(\hat{\theta}, \hat{s}_l, \hat{s}_w)$  represent two convolution kernels (defined in Eq. (5)) that share the same combination coefficients  $w$ , but have different transformation parameters.  $R$  and  $\hat{R}$  denote the convolution outputs of rain map  $M$  with  $C(\theta, s_l, s_w)$  and  $C(\hat{\theta}, \hat{s}_l, \hat{s}_w)$ , respectively.

transformation of the basis functions, that is:

$$\tilde{\phi}(x, \Omega) = \tilde{\phi}(T_\Omega \cdot x) = \sum_{n=1}^N w_n \varphi_n(T_\Omega \cdot x), \quad (4)$$

where  $T_\Omega$  is the inverse transformation matrix with parameter set  $\Omega$ . Then, the discretization of continuous transformable convolution kernel is

$$[\phi(\Omega)]_{ij} = \tilde{\phi}(x_{ij}, \Omega) = \sum_{n=1}^N w_n \varphi_n(T_\Omega \cdot x_{ij}), \quad (5)$$

It should be noted that  $w_n, n = 1, \dots, N$  are learnable parameters when utilizing this convolution kernel in deep CNNs.

**Transformable convolution.** Since  $\phi(\Omega)$  is a  $p \times p$  matrix, which can be viewed as a discrete convolution kernel, we can exploit the common convolution between  $\phi(\Omega)$  and any feature map to perform transformable convolution in the discrete domain. That is,

$$F_{out}(\Omega) = F_{in} \otimes \phi(\Omega), \quad (6)$$

where  $F_{in}$  and  $F_{out}$  represent the input and output feature maps, respectively, and  $\otimes$  denotes



the discrete convolution operator. For easy understanding, Fig. 3 shows an example where the input is the rain map  $M$  and the output is the controllable rain layer  $R$ .

Specifically, in this paper, we will need the rotation and scale transformations. For rotation transformation only, we have  $\Omega = \{\theta\}$ , where  $\theta$  denotes the rotation degree, and

$$T_{\Omega} = T_{\{\theta\}} = \begin{bmatrix} \cos \theta & -\sin \theta \\ \sin \theta & \cos \theta \end{bmatrix}, \quad (7)$$

When we need rotation and scale transformations simultaneously, we can set  $\Omega = \{\theta, s_l, s_w\}$ , and

$$T_{\Omega} = T_{\{\theta, s_l, s_w\}} = \begin{bmatrix} s_w & 0 \\ 0 & s_l \end{bmatrix} \cdot \begin{bmatrix} \cos \theta & -\sin \theta \\ \sin \theta & \cos \theta \end{bmatrix}, \quad (8)$$

where  $\theta, s_l, s_w$  are the rotation degree, the length parameter, and the width parameter, respectively. It should be noted that  $s_l$  and  $s_w$  are actually inversely proportional to the length and width, respectively, since  $T$  is an inverse transformation matrix. In addition, we can find that all parameters (including transform parameters  $\Omega$  and coefficient parameters  $w_n$ ) of the convolution operation defined in Eq. (6) are easy to implement gradient backpropagation in deep learning frameworks. Therefore, the proposed transformable convolution is potentially applicable to a wider range of the architecture designs in deep networks.

## 4 Transformable Rain Generator

The physical rendering based artificial synthesis method shown in Fig. 1 is one of the most rational rainy image generation frameworks. However, it is difficult to formulate this framework into a learnable mathematical model. As an approximation, previous works [38, 39] proposed a convolution sparse coding (CSC) based rain generation model:

$$\mathcal{X} = \mathcal{R} + \mathcal{B} = \tilde{\mathcal{C}} \otimes \tilde{\mathcal{M}} + \mathcal{B}, \quad (9)$$

where  $\mathcal{X}, \mathcal{R}, \mathcal{B} \in \mathbb{R}^{H \times W \times 3}$  are RGB images, denoting the rainy image, the rain layer image, and the clean background image, respectively.  $\tilde{\mathcal{C}} \in \mathbb{R}^{p \times p \times 3 \times K}$  is a rain kernel tensor, representing  $K$  rain kernels,  $\tilde{\mathcal{M}} \in \mathbb{R}^{H \times W \times K}$  denotes  $K$  rain maps,  $H$  and  $W$  represent the height and width of

the images, respectively, and  $p$  denotes the spatial size of the rain kernel. Although  $\tilde{\mathcal{C}}$  and  $\tilde{\mathcal{M}}$  can be learned or generated by deep learning based manners, they are all fixed after the model is trained, which neglects essential dynamic rain factors like shape, orientation, length and so on. Therefore, the model (9) is actually only suitable in deraining tasks, but not suitable for generating rainy images with diverse rain factors. Besides, this model simply adds the rain layer to the background image, which is also just a rough approximation to the real complex situations with fog-like rains.

In the following, we first introduce the proposed rain model, which fully takes necessary rain streak factors, including the shape, orientation, length, width and sparsity, into consideration. Then we present the proposed transformable rainy image generator, which takes the proposed rain model as the backbone. Lastly, we describe the training strategy and implementation details for the rainy image generator.

### 4.1 Proposed Backbone Rain Model

Although the artificial synthesis method shown in Fig. 1 is difficult to be mathematically formulated with traditional convolution operators, it is actually not hard to be properly modeled with the proposed transformable convolution operator. Following the pipeline of Fig. 1, we encode the shape, orientation, length, width factors of the rain into the transformable rain kernel, and encode the sparsity factor into the rain map. The expected rain model is expressed as:

$$\begin{aligned} \mathcal{X}(\theta, s_l, s_w, \boldsymbol{\alpha}, \tau) &= \text{MerNet}(\mathcal{R}(\theta, s_l, s_w, \boldsymbol{\alpha}, \tau), \mathcal{B}) \\ &= \text{MerNet}(\mathcal{C}(\theta, s_l, s_w, \boldsymbol{\alpha}) \otimes \mathcal{M}(\tau), \mathcal{B}), \end{aligned} \quad (10)$$

where  $\theta, s_l, s_w, \boldsymbol{\alpha}$  and  $\tau$  represent the orientation, length, width, shape, and sparsity parameters, respectively.  $\mathcal{X}(\theta, s_l, s_w, \boldsymbol{\alpha}, \tau)$ ,  $\mathcal{R}(\theta, s_l, s_w, \boldsymbol{\alpha}, \tau)$  and  $\mathcal{B}$  denote the parameterized rainy image, the parameterized rain layer and the input clean background image, respectively.  $\mathcal{C}(\theta, s_l, s_w, \boldsymbol{\alpha}) \in \mathbb{R}^{p \times p \times 3 \times K}$  and  $\mathcal{M}(\tau) \in \mathbb{R}^{H \times W \times K}$  are the rain kernel and the rain map, corresponding to  $\tilde{\mathcal{C}}$  and  $\tilde{\mathcal{M}}$  in Eq. (9), respectively. MerNet( $\cdot$ ) is a deep network for merging the rain layer and background image, which simulates the interaction between



multiplication along the  $4^{th}$  dimension<sup>4</sup>. Besides,  $\mathcal{D}(\theta, s_l, s_w)$  is parameterized with the manner in Eq. (5). By substituting Eqs. (5) and (8), we can obtain that for any  $i, j = 1, 2, \dots, p$ ,  $c = 1, 2, 3$  and  $k = 1, 2, \dots, K$ ,

$$\begin{aligned} & [\mathcal{C}(\theta, s_l, s_w, \alpha)]_{ijck} \\ &= \sum_{mn} \alpha_{mk} \cdot w_{mnc}^d \cdot \varphi_n(T_{\{\theta, s_l, s_w\}} \cdot x_{ij}), \end{aligned} \quad (12)$$

where  $\{\varphi_n\}_{n=1}^N$  are the basis functions defined in Eqs. (2) and (3), and the tensor  $\mathbf{w}^d \in \mathbb{R}^{M \times N \times 3}$  denotes the to-be-learned coefficient parameters for the rain kernel dictionary.

**Rain kernel generator.** It is easy to find that the calculation about  $\theta, s_l, s_w$  and  $\alpha$  only involves simple operations, all of which can be easily performed using popular deep learning tools, such as Pytorch, Tensorflow, and general gradient backpropagation algorithms. Therefore, we can adopt lightweight fully connection networks (FCNs) for learning the distribution of these parameters, and train these FCNs with other parts of the proposed rainy image generator in an end-to-end way. Specifically, as shown in Fig. 4 (a), we exploit the following four FCNs for rain factors generation<sup>5</sup>:

$$\begin{cases} \theta = \text{FCN}_{\mathbf{w}^\theta}^\theta(e_\theta), & e_\theta \sim N(0, 1), \\ s_l = \text{FCN}_{\mathbf{w}^l}^l(e_l), & e_l \sim N(0, 1), \\ s_w = \text{FCN}_{\mathbf{w}^w}^w(e_w), & e_w \sim N(0, 1), \\ \alpha = \text{FCN}_{\mathbf{w}^\alpha}^\alpha(e_\alpha), & e_\alpha \sim N(0, 1), \end{cases} \quad (13)$$

where all FCNs are input with Gaussian noise, and  $\mathbf{w}^\theta, \mathbf{w}^l, \mathbf{w}^w$  and  $\mathbf{w}^\alpha$  denote the to-be-learned parameters of the FCNs. Combining Eqs. (12) and (13), the entire rain kernel generator is

$$\begin{aligned} \mathcal{C}_{ijck} &= \sum_{mn} w_{mnc}^d \cdot [\text{FCN}_{\mathbf{w}^\alpha}^\alpha(e_\alpha)]_{mk} \cdot \\ & \varphi_n \left( T_{\{\text{FCN}_{\mathbf{w}^\theta}^\theta(e_\theta), \text{FCN}_{\mathbf{w}^l}^l(e_l), \text{FCN}_{\mathbf{w}^w}^w(e_w)\}} x_{ij} \right), \end{aligned} \quad (14)$$

where  $\mathcal{C} \in \mathbb{R}^{p \times p \times 3 \times K}$  is the output rain kernel, and  $\{e_\theta, e_l, e_w, e_\alpha\} \sim N(0, 1)$ . One can refer to Fig. 4 (a) for an easy understanding of the rain kernel generator (14). For conciseness, we more

briefly rewrite Eq. (14) as:

$$\mathcal{C} = \text{KerNet}_{\mathbf{w}^c}(e_\theta, e_l, e_w, e_\alpha), \quad (15)$$

where  $\mathbf{w}^c = \{\mathbf{w}^d, \mathbf{w}^\theta, \mathbf{w}^l, \mathbf{w}^w, \mathbf{w}^\alpha\}$  is all to-be-learned parameters for rain kernel generation, which can be easily trained with off-the-shelf gradient backpropagation algorithms.

## 4.2.2 Rain map Generation

**Rain map model.** The rain map  $\mathcal{M}(\tau, \theta)$  mainly controls the position and sparsity of rain streaks. There are two key issues to be solved here: the first one is how to embed the orientation factor  $\theta$  into the rain map model and make the rain map consistent with the rotation of the rain kernel; the second one is how to embed the sparsity parameter  $\tau$  into the model. For the first issue, we introduce a rotatable ResNet (rotResNet), which is defined by replacing all the convolution kernels in the commonly used ResNet[40] with the proposed rotatable convolution kernels defined in Eq. (5). Formally, we have

$$\text{rotResNet}_{\mathbf{w}^r}(\cdot, \theta) = \text{ResNet}_{\phi_{\mathbf{w}^r}(\theta)}(\cdot), \quad (16)$$

where  $\text{ResNet}_{\phi}(\cdot)$  denotes the commonly used ResNet whose convolution kernel is denoted by  $\phi$ , and  $\phi_{\mathbf{w}^r}(\theta)$  is the parameterized convolution kernel defined by Eqs. (5) and (7), i.e.,  $(\phi_{\mathbf{w}^r}(\theta))_{ij} = \sum_{n=1}^N w_n^r \varphi_n(T_{\{\theta\}} \cdot x_{ij})$ .  $\text{rotResNet}_{\mathbf{w}^r}(\cdot, \theta)$  represents the rotatable ResNet with the rotation degree  $\theta$  and the coefficient parameters  $\mathbf{w}^r$ .

For the second issue, a threshold ReLU operator is introduced for controlling the sparsity of rains. As a result, the proposed rain map model is

$$\mathcal{M}(\tau, \theta) = \text{ReLU}(\text{rotResNet}_{\mathbf{w}^r}(\mathcal{Z}, \theta) - \tau), \quad (17)$$

where  $\text{ReLU}(\cdot)$  denotes the ReLU activate function [41], and  $\tau$  represents the sparsity factor of rain. It's easy to see that the larger  $\tau$  is, the more sparse the rain map will be.  $\mathcal{Z} \in \mathbb{R}^{H \times W \times K}$  is the input random Gaussian noise.  $\theta$  is the orientation degree, which is defined in Eq. (13).

**Rain map generator.** Similar Eq. (13) for learning other rain factors, we adopt a lightweight FCN to learn the distribution of sparsity factor  $\tau$ :

$$\tau = \text{FCN}_{\mathbf{w}^\tau}^\tau(e_\tau), \quad e_\tau \sim N(0, 1), \quad (18)$$

<sup>4</sup>For  $\mathcal{D} \in \mathbb{R}^{p \times p \times 3 \times M}$  and  $\alpha \in \mathbb{R}^{M \times K}$ ,  $(\mathcal{D} \odot \alpha) \in \mathbb{R}^{p \times p \times 3 \times K}$  and  $(\mathcal{D} \odot \alpha)_{\{:::,:::,k\}} = \sum_{m=1}^M \mathcal{D}_{\{:::,:::,m\}} \alpha_{mk}$ .

<sup>5</sup>There is a reshape in output of the FCN for  $\alpha$ .



where  $\mathbf{w}^\tau$  denotes the to-be-learned parameters. By substituting Eqs. (13) (18) into (17), we can obtain the entire rain map generator:

$$\mathcal{M} = \text{ReLU}\left(\text{rotResNet}_{\mathbf{w}^\tau}\left(\mathcal{Z}, \text{FCN}_{\mathbf{w}^\theta}^\theta(e_\theta)\right) - \text{FCN}_{\mathbf{w}^\tau}^\tau(e_\tau)\right), \quad (19)$$

where  $\mathcal{M} \in \mathbb{R}^{H \times W \times K}$  is the output rain map, and  $\{\mathcal{Z}, e_\theta, e_\tau\} \sim N(0, 1)$  are the input Gaussian noise.  $\mathbf{w}^\theta$  and  $e_\theta$  are shared with Eq. (15). One can refer to Fig. 4 (b) for better understanding. For simplicity, we rewrite Eq. (19) as:

$$\mathcal{M} = \text{MapNet}_{\mathbf{w}^m}(\mathcal{Z}, e_\tau, e_\theta), \quad (20)$$

where  $\mathbf{w}^m = \{\mathbf{w}^r, \mathbf{w}^\tau, \mathbf{w}^\theta\}$  represents all the to-be-learned parameters.

### 4.2.3 Merging Rain Layer and Background

**Merging model.** For the merging network  $\text{MerNet}(\cdot)$  in Eq. (10), we use a deep CNN for simulating the interaction between rain layer and the rainless background. Similar to the aforementioned rain map generator, we also adopt rotatable ResNet for the merging model, in order to be consistent with the rotation of the rain kernel. Formally, the merging model is

$$\mathcal{X}(\theta, s_l, s_w, \boldsymbol{\alpha}, \tau) = \text{rotResNet}_{\mathbf{w}^o}(\text{cat}(\mathcal{R}(\theta, s_l, s_w, \boldsymbol{\alpha}, \tau), \mathcal{B}), \theta), \quad (21)$$

where  $\text{rotResNet}_{\mathbf{w}^o}(\cdot, \theta)$  denotes the rotatable ResNet defined in Eq. (16) with  $\mathbf{w}^o$  denoting the to-be-learned parameters.  $\text{cat}(\cdot)$  represents the concatenation along the 3<sup>rd</sup> dimension.  $\mathcal{R}(\theta, s_l, s_w, \boldsymbol{\alpha}, \tau) = \mathcal{C}(\theta, s_l, s_w, \boldsymbol{\alpha}) \otimes \mathcal{M}(\tau, \theta)$  is the parameterized rain layer. We can see that the model (21) is actually an executable version of the rainy image model (10).

**Merging network.** Combining model (21) with the FCN for  $\theta$  in Eq. (13), we can obtain the entire merging network:

$$\mathcal{X} = \text{rotResNet}_{\mathbf{w}^o}\left(\text{cat}(\mathcal{R}, \mathcal{B}), \text{FCN}_{\mathbf{w}^\theta}^\theta(e_\theta)\right), \quad (22)$$

where  $\mathbf{w}^\theta$  and  $e_\theta$  are shared with Eqs. (14) and (19). Please refer to Fig. 4 (c) for a better

understanding of this design. We can then more concisely rewrite Eq. (22) as:

$$\mathcal{X} = \text{MerNet}_{\mathbf{w}^x}(\mathcal{R}, \mathcal{B}, e_\theta), \quad (23)$$

where  $\mathbf{w}^x = \{\mathbf{w}^o, \mathbf{w}^\theta\}$  denotes the to-be-learned parameters for merging network.

**Rainy image generator.** By substituting Eqs. (15), (20) and (23) into the backbone model (10), the proposed rainy image generator is

$$\begin{aligned} \mathcal{X} &= \text{TRG-Net}_{\mathbf{w}}(\mathcal{B}, \mathcal{Z}, e) \\ &\triangleq \text{MerNet}_{\mathbf{w}^x}(\text{KerNet}_{\mathbf{w}^c}(e_\theta, e_l, e_w, e_\alpha) \otimes \text{MapNet}_{\mathbf{w}^m}(\mathcal{Z}, e_\tau, e_\theta), \mathcal{B}, e_\theta). \end{aligned} \quad (24)$$

where  $\mathbf{w} = \{\mathbf{w}^x, \mathbf{w}^c, \mathbf{w}^m\}$  represents all the to-be-learned parameters and  $e = \{e_\theta, e_l, e_w, e_\alpha, e_\tau\} \sim N(0, 1)$ . For brevity, we name this transformable rainy image generation network as TRG-Net.

**Remark.** It should be noted that the proposed framework not only possesses intrinsic interpretability, where the distribution of rain factors can be purely learned from data using GAN-based manners, but also has essential controllability. Specifically, after achieving  $\mathbf{w}$  through learning from data, we can obtain all parameters. Then either manually-set rain factors or FCN-generated rain factors can be utilized as the inputs to model (21). When using manually-set rain factors, the generated rainy images are essentially controlled. These merits are finely validated in Fig. 7 below.

### 4.3 Loss Function

To capture the rain distribution in a real scene, the adversarial training strategy [15] is applied to train TRG-Net. The basic loss function is:

$$\mathcal{L}_{adv}(\text{TRG-Net}_{\mathbf{w}}(\mathcal{B}, \mathcal{Z}, e), \mathcal{X}_0) + \lambda L_{rotTV}, \quad (25)$$

where  $\mathcal{L}_{adv}$  is the GAN loss.  $\mathcal{X}_0$  denotes the adversarial rainy image in training set.  $\lambda$  is the trade-off parameter, and  $L_{rotTV}$  represents specifically proposed regularizer for the task, which will be introduced in the following.

#### Rotatable Total Variation Regularizer.

Traditional total variation regularizer adopts the sparsity penalty on the first-order differential field of an image, which is in respect to the fact that most local parts of an image are smooth and

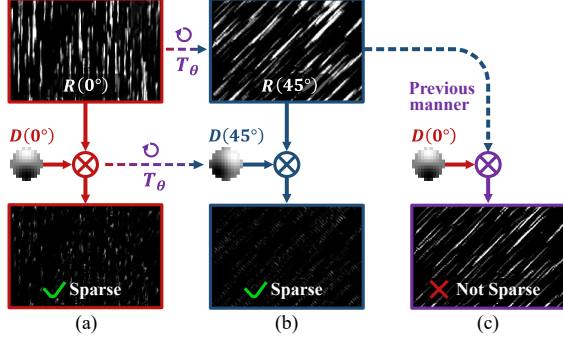


**Fig. 5** The differential field of a rain layer along its rain streak orientation is significantly sparser than those along other orientations. (a) The differential field of the rain  $R(0^\circ)$  with  $0^\circ$  orientation along the  $0^\circ$  orientation is sparse. (b) The differential field of the rain  $R(45^\circ)$  with  $45^\circ$  orientation along the  $45^\circ$  orientation is also sparse. (c) The differential field of the rain  $R(45^\circ)$  with  $45^\circ$  orientation along the  $0^\circ$  orientation is not sparse.

edges in a natural image are sparse. Formally, TV regularizer can be presented as:

$$L_{\text{TV}} = \|\hat{D} \otimes \hat{\mathcal{X}}\|_1, \quad (26)$$

where  $\hat{D}$  denotes the first-order difference filter and  $\hat{\mathcal{X}}$  is an input image. It has been shown that TV regularizer is greatly helpful to improve the performance in many tasks [42–44].

However, the first order differential field of the rain layer is generally very anisotropic, where the differential field along the rain streak orientation can be significantly sparser than those along other orientations [45, 46] (as shown in Fig. 5). This fact yields the requirement of higher penalty along the rain streak orientation. Therefore, there is obvious room to improve the TV regularizer in rain layer regularization, since the difference filter  $\hat{D}$  in the traditional TV regularizer can hardly be flexibly rotated to finely adapt different orientations of rain streaks in different images.

Fortunately, in the proposed method, the orientation degree  $\theta$  of the generated rain layer is able to be readily extracted by our model without extra effort. Moreover, the proposed filter parameterization and transformable convolution techniques allow us to design a rotated differential filter. By adopting the transformable kernel (5) and the inverse rotation matrix (7), the proposed rotated differential filter can be naturally defined.

For  $\forall i, j = 1, 2, \dots, p$ , we have

$$[D(\theta)]_{ij} = \sum_{n=1}^N w_n \varphi_n(T_{\{\theta\}} \cdot x_{ij}), \quad (27)$$

Then, we can estimate  $w_n$  by solving  $D(0) = \hat{D}$ , where  $\hat{D}$  is the vertical difference filter. That is, we need to solve the following linear equation:

$$\sum_{n=1}^N w_n \varphi_n(x_{ij}) = \hat{D}_{ij}, \forall i, j = 1, 2, \dots, p, \quad (28)$$

Actually, the solution to this equation is quite simple. Since FSE-FP used in our model is equivalent to the discrete inverse Fourier transform when  $\theta = 0$ ,  $w_n$  can be solved by adopting discrete Fourier transform on  $\hat{D}_{ij}$ , i.e.,  $w_n = 1/p^2 \sum_{st} \hat{D}_{st} \varphi_n(x_{st})$ . Then  $\forall i, j = 1, 2, \dots, p$ , we have

$$[D(\theta)]_{ij} = \frac{1}{p^2} \sum_{nst} \hat{D}_{st} \cdot \varphi_n(x_{st}) \cdot \varphi_n(T_{\{\theta\}} \cdot x_{ij}), \quad (29)$$

Then the proposed rotatable total variation (rotTV) regularizer can be explicitly calculated by

$$L_{\text{rotTV}} = \|D(\theta) \otimes \mathcal{R}\|_1. \quad (30)$$

In this paper, when we add this regularizer to the basic loss function,  $\mathcal{R}$  is set as the generated rain layer (defined in Eq. (10)), and  $\theta = \text{FCN}_{\mathbf{w}\theta}^\theta(e_\theta)$  and  $\lambda$  is empirically set as 1. It is easy to see that the calculation that is caused by this term is readily backpropagated in deep networks.

#### 4.4 Implementation Details

In order to adapt the rainy images to practical scenarios, where the orientations of rain streaks in a rainy image may be inconsistent, we can set  $\theta$  as a vector with  $M$  elements instead of a scalar (i.e., setting the output dimension number of  $\text{FCN}_{\mathbf{w}\theta}^\theta$  as  $M$  instead of 1), where each element in this orientation vector represents an individual orientation of the element in the rain kernel dictionary.

Our experiments empirically show that a single convolution of the rain kernel and the rain map is usually not sufficient to generate the diverse, complex and long rain streaks. Therefore, we actually generate three rain kernels and convolute them

with the rain maps to increase the receptive field of rain kernel.

Besides, it is easy to find that the rain kernels contain a clear physical meaning, which is quite different from other convolution kernels in deep networks. Therefore, we specifically design an initialization manner for them, which achieves a streak-like initialization. Please refer to the appendix for more details for the rain kernels initialization and generation.

The number of rain kernel dictionary  $M$  and the number of rain maps  $K$  are set as 30 and 6, respectively. The size of rain kernels is  $11 \times 11$ . For most of our experiments, we simply utilize 2 and 4 resblocks in the rain map model and the merging model, respectively. For datasets with heavy fog (i.e., Kitti [30]), a deeper merging model (with 10 resblocks) is employed to simulate the fog. Actually, more complex structures can be designed for these two parts based on actual needs in practice.

## 5 Experimental Results

In this section, we first validate the learning ability of the proposed rain generator and its controllability with respect to rain factors. Then, we comprehensively demonstrate the superiority of the proposed method in the sense of the quality of the generated samples, based on a series of experiments, including unpaired rain generation and paired rain augmentation, by comparison with the SOTA rainy image generators, e.g., VRG-Net [18].

### 5.1 Rain Generator Verification

The proposed rain generator learns the rain factors by FCNs from data samples. This allows us to extract their distributions purely from the rain data set. We thus verify this capability on Rain100L [27], a synthetic rain dataset containing 200 pairs of rainy and rainless images for training.

**Experiment settings.** To train TRG-Net by an adversarial strategy, following [22] and [35], we adopt a patch-based discriminator [17]. Following [18], the initial learning rates for the generator and the discriminator are  $1 \times 10^{-4}$  and  $4 \times 10^{-4}$ , respectively. As suggested in [47], we update the discriminator five times for each generator updating. We utilize Adam algorithm [48] to optimize the rain generation network. We train the proposed generator for 200 epochs with rotatable TV

regularizer, and the network is trained for 3000 iterations in each epoch. We randomly crop a  $256 \times 256$  patch as input in each iteration.

**Rain Generator Verification.** Fig. 6 depicts the rain generation process in a paired training manner on Rain100L for both VRG-Net [18] and the proposed TRG-Net. One can see easily that the rain randomly initialized by TRG-Net already exhibits some rain patterns due to the embedding of a reasonable rain model, whereas the rain initialized by VRG-Net [18] appears to be mere noise. Furthermore, the rain generated by TRG-Net displays clear rain streaks even in the first epoch. These observations suggest that TRG-Net may exhibit relatively higher quality rain and a faster convergence rate for rain generation compared to VRG-Net, which will be further validated in subsequent experiments.

The learned distributions<sup>6</sup> of rain factors in Rain100L are shown in Fig. 7, which can be easily used to further generate different rain types by adjusting rain factors in a controllable manner. As shown in Fig. 7 (a), the learned orientation degree  $\theta$  distribution is close to a Gaussian distribution, with values mostly between  $-40$  and  $40$ , which complies with the intuitive orientation distribution in Rain100L [5]. By model (21), we can manually input the orientation degree into the trained generator to control the orientation of the generated rain steaks. Fig. 7 (a) shows the rain generated with input  $\theta$  of  $0^\circ$ ,  $30^\circ$ ,  $60^\circ$ ,  $-30^\circ$ , respectively. It should be noted that this manner offers the capability to generate OOD rains, e.g., the  $60^\circ$  rain in Fig. 7 (a), which will be beneficial for deraining on OOD rain data sets (see OOD rain augmentation in Sec. 5.3.3). Yet this is difficult to be achieved by traditional DL-based generators, since black-box model can hardly generalize samples beyond the distribution of training data. Similarly, in Fig. 7 (b), (c) and (d), we can observe that the proposed method can also learn the distributions of  $s_l$ ,  $s_w$  and  $\tau$ , respectively. We can control rain from thin to thick and from short to long by scaling the rain kernels according to different  $s_w$  and  $s_l$  values, respectively, and control the sparsity of rain by adjusting the input of  $\tau$ .

---

<sup>6</sup>The distribution is approximated by the histogram obtained by sampling 10000 times.

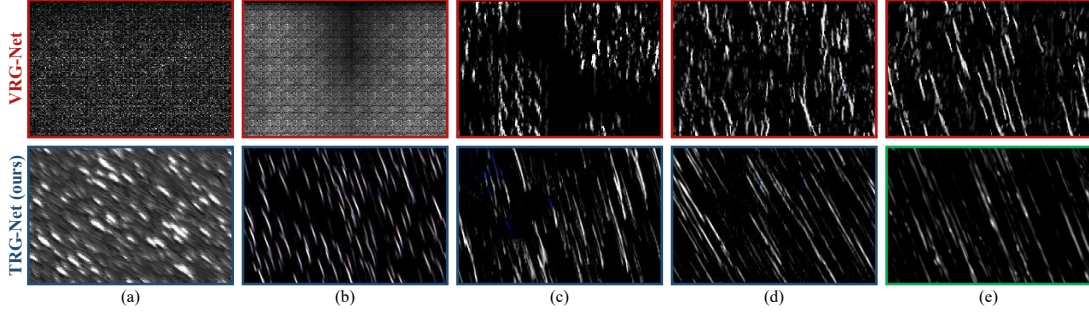
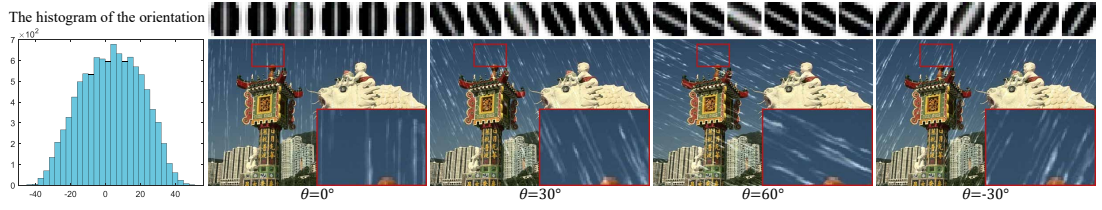
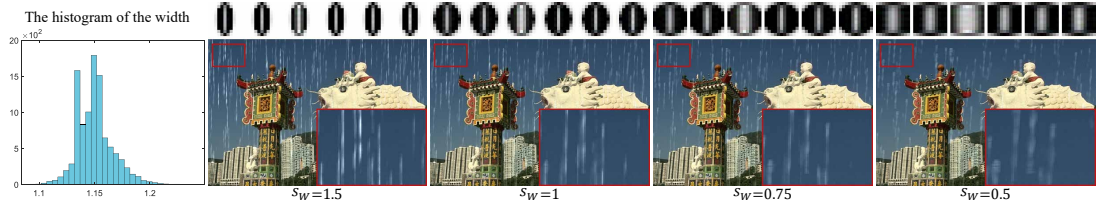


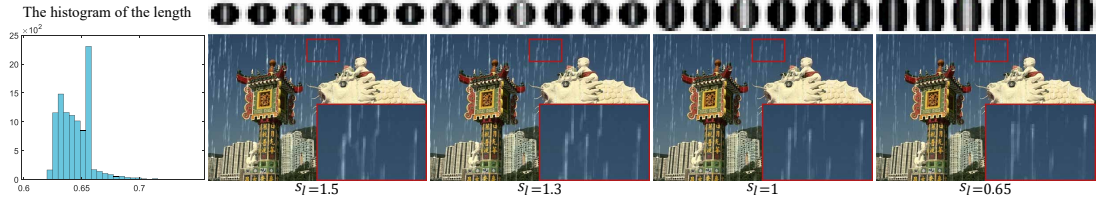
**Fig. 6** The rain generation process on Rain100L in a paired training manner for both VRG-Net [18] and the proposed TRG-Net. (a)-(d): The rain generated by VRG-Net [18] (upper) and the proposed TRG-Net (lower) at random initialization, 1st, 10th and 60th epochs, respectively. (e) The rain generated by VRG-Net [18] at 700th epoch (upper) and a typical reference rain in Rain100L [27] (lower).



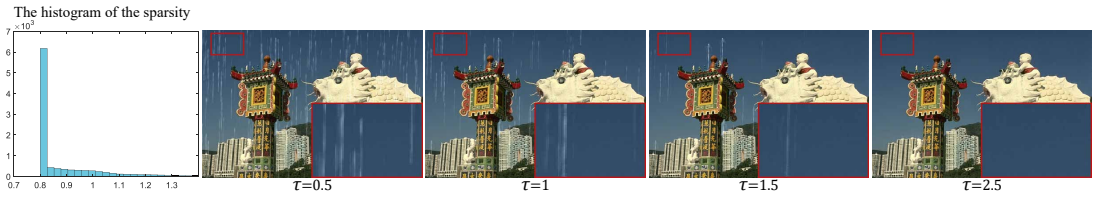
(a) The extracted orientation  $\theta$  distribution from Rain100L. The right four columns show the rainy images generated by inputting different orientation degree  $\theta$  into TRG-Net.



(b) The learned distribution of width  $s_w$  in Rain100L, whose values are all around 1.15. The right four columns show the rainy images generated by inputting different width parameters  $s_w$  into TRG-Net.



(c) The learned length  $s_l$  distribution from Rain100L, with values mostly between 0.6 and 0.7. The right four columns show the rainy images generated by inputting different length parameter  $s_l$  into TRG-Net.



(d) The obtained sparsity  $\tau$  distribution in Rain100L. The right four columns show the rainy images generated by inputting different sparsity parameter  $\tau$  into TRG-Net.

**Fig. 7** The learned distributions of rain factors in Rain100L by the proposed TRG-Net, which enables to generate different types of rains by adjusting these rain factors in a controlled manner. (a)-(d) The first column are the learned distributions with respect to the orientation degree, width, length and sparsity, respectively, and the right four columns are some different rain types generated by adjusting these factors.



**Table 1** The FID and KID of unpaired rain generation on four rain datasets. **Bold** indicates the best result.

Datasets	VRG-Net [18]		TRG-Net	
	FID	KID	FID	KID
Rain100L	61.18	0.0196	<b>25.78</b>	<b>0.0047</b>
Cityscapes	39.94	0.0306	<b>20.34</b>	<b>0.0133</b>
Kitti	56.98	<b>0.0364</b>	<b>51.44</b>	0.0392
SPA-Data	68.34	0.0391	<b>48.79</b>	<b>0.0204</b>

## 5.2 Unpaired Rain Generation

In this section, we first conduct unpaired rain generation on three synthetic rain datasets and a real rain dataset. Then deraining experiments on the pseudo-paired data generated by the rain generators are performed to evaluate the quality of the unpaired generated rainy images for deraining.

### 5.2.1 Unpaired Rain Generation

**Experiment settings.** We perform unpaired rain generation on three synthetic rain datasets, Rain100L, Cityscapes [30] and Kitti<sup>7</sup> [30], and a real rain dataset, SPA-Data [25], to verify the superiority of our rain generator. Specifically, to construct a complete unpaired training dataset, we remove the rainless images of half of the data samples and remove the rainy images of the other half of the data samples. The rotatable TV regularizer is used for the training of Rain100L. The generator is trained for 400 epochs on Cityscapes and Kitti, and 30 epochs and 250 epochs on Rain100L and SPA-Data, respectively. The same patch-based discriminator [17] is employed for all generators. Inspired by [52], we use the high frequency components of the rainy images instead of the rainy image itself as input to the discriminator for better discrimination. The other training settings are the same as those used in Sec. 5.1. We utilize Fréchet Inception Distance (FID) and Kernel Inception Distance (KID) as metrics for assessing the quality of generated rainy images, where lower values indicate better performance.

<sup>7</sup>The rains in Cityscapes and Kitti are synthesised [30] with varying rainfall rate to evaluate the effect of rain on computer vision tasks in the outdoor environment, which consider the imaging mechanism, such as fog-like attenuation and rain photometry, under the condition of camera motion. For them, we select the 100mm/hr rain as training set and test set in this experiment. As the rain orientations in Cityscapes and Kitti are correlated with the position, we have further included three learnable masks on the rain maps to distinguish different orientations in different positions for the two datasets.

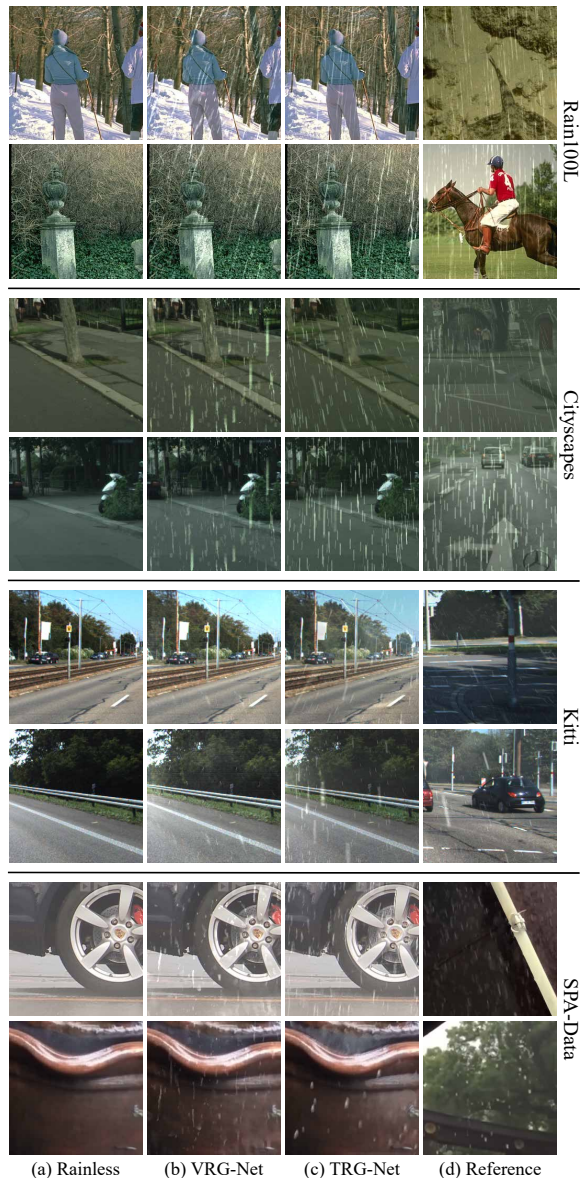


**Fig. 8** The results of unpaired rain generation by VRG-Net and the proposed TRG-Net on three synthetic datasets and a real dataset. (a)-(d) are the rainless background images, the rainy images generated by VRG-Net, the rainy images generated by the proposed TRG-Net and the reference rainy images which are used for unpaired training, respectively. Every dataset displays two generated samples.

**Experimental results.** Table 1 shows the FID and KID results on four datasets. Our model achieves lower FID and KID compared to VRG-Net on all datasets, excepting the KID on Kitti, which means that the rainy images generated by



**Table 2** The quantitative results of all competing methods on synthetic and real datasets. A\* indicates the deraining results of PReNet [32] trained on the pseudo-paired data generated by method A. The best result is highlighted with **bold**.

Methods	Rain100L		Cityscapes		Kitti		SPA-Data	
	PSNR	SSIM	PSNR	SSIM	PSNR	SSIM	PSNR	SSIM
DSC [49]	27.34	0.849	21.63	0.778	19.46	0.892	34.83	0.941
JCAS [50]	28.54	0.852	22.63	0.877	18.92	0.867	34.95	<b>0.945</b>
CycleGAN [16]	22.56	0.771	23.37	0.836	30.87	0.943	24.26	0.879
DerainCycleGAN [21]	28.93	0.906	22.17	0.882	21.78	0.912	29.96	0.904
DCD-GAN [22]	19.81	0.700	21.57	0.674	24.88	0.826	15.58	0.624
CycleGAN [16]*	25.11	0.832	22.62	0.908	26.88	0.937	22.71	0.866
DerainCycleGAN [21]*	28.50	0.910	21.10	0.871	22.31	0.938	22.01	0.863
DCD-GAN [22]*	22.48	0.821	19.84	0.850	23.55	0.903	19.81	0.786
VRG-Net [18]*	27.84	0.855	21.94	0.768	21.08	0.906	34.81	0.931
TRG-Net*	<b>32.33</b>	<b>0.949</b>	<b>24.86</b>	<b>0.959</b>	<b>32.15</b>	<b>0.983</b>	<b>35.80</b>	<b>0.945</b>

**Table 3** The segmentation performance of all competing methods on Cityscapes. **Bold** is the best result.

Methods	mIoU	mAcc
Rain	37.30	50.61
DSC [49]	28.82	39.12
JCAS [50]	43.74	57.35
CycleGAN [16]	40.85	54.13
DerainCycleGAN [21]	48.61	61.36
DCD-GAN [22]	29.89	40.57
CycleGAN [16]*	50.86	64.38
DerainCycleGAN [21]*	48.74	64.96
DCD-GAN [22]*	44.21	60.02
VRG-Net [18]*	36.99	50.28
TRG-Net*	<b>66.57</b>	<b>76.85</b>
Clean (Upper bound)	72.50	80.82

the proposed TRG-Net has a higher rain quality than VRG-Net [18] and is able to capture the rain generation mechanism under different environment conditions. In Fig. 8, we show some typical results of the unpaired rain generation. It is easy to observe that the rain streaks generated by VRG-Net, which represents the CNN-based method, could be largely lacking in diversity, for example, the rain streaks in two random generation results on different background images are very similar, as shown in Fig. 8 (b). In contrast, the rainy images generated by the proposed TRG-Net not only better resemble to the original rainy images in their underlying rain patterns, i.e. the physical factors of rain such as shape and photometry are finely captured by our model, but also achieve more diversity in rain factors, such as orientation, length, width and sparsity. Actually, the

diversity in rain factors of TRG-Net is easy to understand, and we can observe from Fig. 7 that TRG-Net has extracted a specific distribution for rain factors, which certainly leads to the diversity in these factors. These results clearly substantiate the superiority of the proposed TRG-Net over the previous method.

### 5.2.2 The Effectiveness of the Unpaired Generated Data for Deraining

To demonstrate the effectiveness of the unpaired generated rainy images for deraining, we perform deraining experiments using the pseudo-paired data generated by the rain generators as the training data of deraining networks.

**Experiment settings.** We adopt PReNet [32], a simple deraining baseline, as the derainer to demonstrate the effectiveness of the generated pseudo train data sets for deraining. The training pairs for PReNet consist of rainless images from the train dataset of the unpaired rain generation experiment and their corresponding pseudo-paired rainy images generated by the rain generators. The competing unpaired methods include the model-based methods, DSC [49] and JCAS [50], and the DL-based methods, CycleGAN [16], DerainCycleGAN [21] and DCD-GAN [22]. Since the DL-based unpaired methods here are all CycleGAN-based framework which can also generate pseudo rainy images, we also train PReNet using the pseudo-paired data generated by these methods, for a fair comparison between these methods and rain generation methods. For

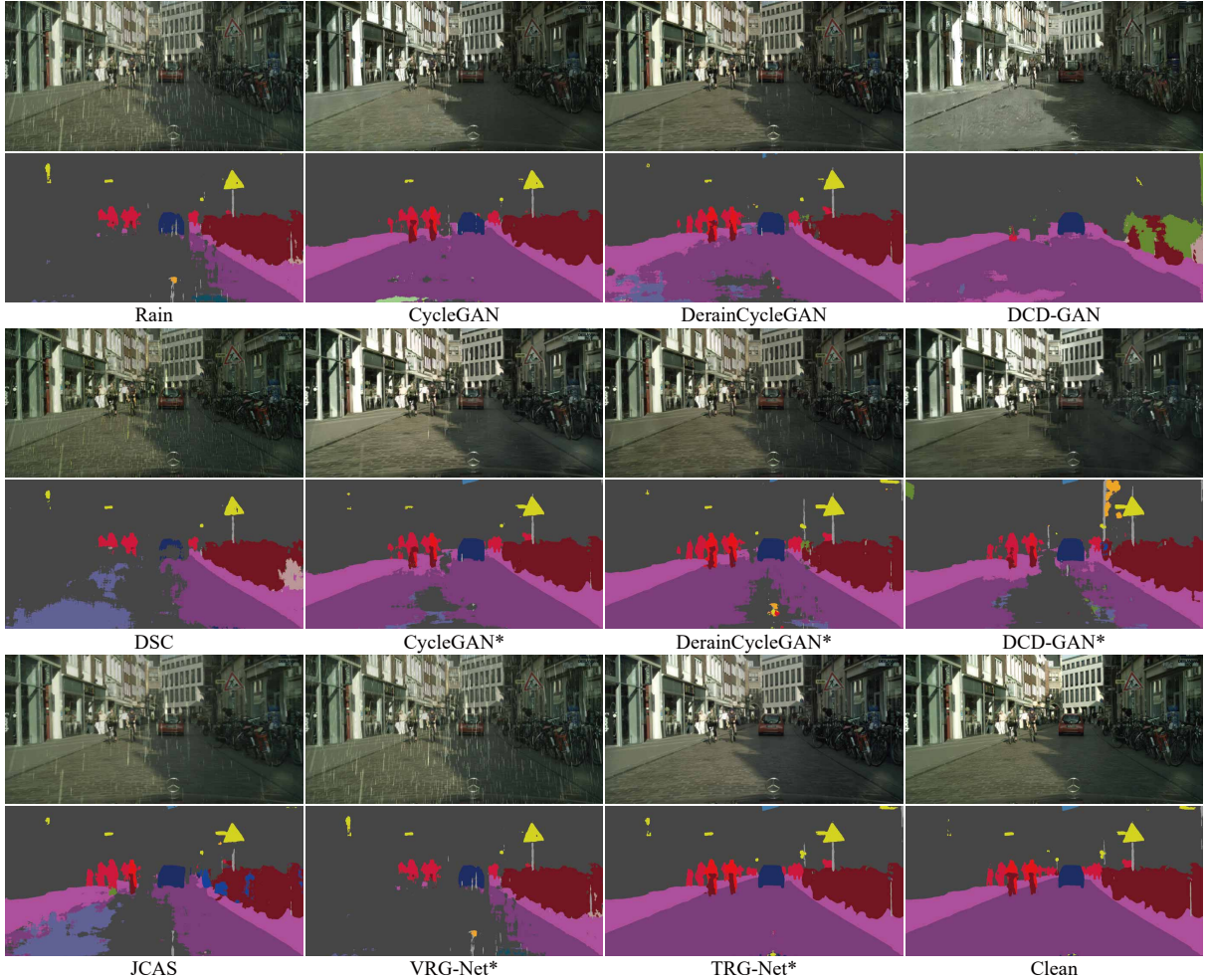


**Fig. 9** The deraining results (the first row in each group) of all competing methods in an unpaired manner on Cityscapes, and their corresponding semantic segmentation results (the second row in each group) on ERFNet [51].

convenience, we use the notation  $A^*$  to denote the deraining results of PReNet trained on the pseudo paired data generated by method A. Peak-signal-to-noise (PSNR) and structure similarity (SSIM) are used to quantify the deraining performance, which are calculated in Y channel of YCbCr space following previous works [18, 22].

**Experimental results.** Table 2 lists the quantitative results of all competing methods on four datasets. We can observe that TRG-Net\* outperforms all the other competing methods, which demonstrates the superiority of the unpaired generated rainy images by our model for deraining. Besides, to evaluate the effectiveness of unpaired deraining results for downstream tasks, we perform semantic segmentation experiments using ERFNet [51] on Cityscapes. The mean intersection

over union (mIoU) and mean accuracy (mAcc) of the segmentation results are reported in Table 3. Our model obtains the best segmentation performance among all competing methods, which is significantly superior to the segmentation results of rainy images and shows only a small discrepancy when compared to clean images. In Fig. 9, we provide the deraining results of all competing methods on a representative sample of Cityscapes and their corresponding semantic segmentation results. It can be seen that TRG-Net\* consistently achieves evidently superior visual results.

These unpaired experiments demonstrate that the rainy images generated by the proposed rain generation method are not only of higher quality than those generated by the common CCN-based

**Table 4** The deraining results on synthetic datasets. Baseline means the derainers trained on the original dataset without augmentation. VRG-Net and TRG-Net denote augmented training using VRG-Net and the proposed TRG-Net, respectively. **Bold** is the best result.

Datasets	Methods	PReNet		SPANet		JORDER_E		RCDNet		DRSformer	
		PSNR	SSIM	PSNR	SSIM	PSNR	SSIM	PSNR	SSIM	PSNR	SSIM
Rain100L	Baseline	37.43	0.979	35.82	0.972	37.76	0.980	39.83	0.986	40.21	<b>0.987</b>
	VRG-Net	37.79	0.980	36.07	0.973	38.38	0.981	40.05	0.986	40.39	<b>0.987</b>
	TRG-Net	<b>38.16</b>	<b>0.982</b>	<b>36.28</b>	<b>0.974</b>	<b>38.68</b>	<b>0.983</b>	<b>40.30</b>	<b>0.987</b>	<b>40.48</b>	<b>0.987</b>
Rain100L-S	Baseline	36.42	0.974	35.01	0.967	36.47	0.973	39.08	0.984	39.09	0.983
	VRG-Net	36.89	0.976	35.60	<b>0.970</b>	37.30	0.976	39.45	0.985	39.25	0.984
	TRG-Net	<b>37.21</b>	<b>0.978</b>	<b>35.70</b>	<b>0.970</b>	<b>37.50</b>	<b>0.978</b>	<b>39.63</b>	<b>0.986</b>	<b>39.89</b>	<b>0.986</b>
Rain100H	Baseline	30.16	0.908	27.22	0.866	29.80	0.895	31.05	0.909	32.44	<b>0.926</b>
	VRG-Net	<b>30.19</b>	<b>0.909</b>	27.30	0.866	30.20	0.900	<b>31.16</b>	<b>0.911</b>	<b>32.46</b>	0.924
	TRG-Net	30.16	0.908	<b>27.36</b>	<b>0.867</b>	<b>30.33</b>	<b>0.902</b>	31.06	<b>0.911</b>	<b>32.46</b>	0.925
Rain100H-S	Baseline	27.83	0.878	26.53	0.854	27.32	0.864	29.52	0.896	29.62	0.897
	VRG-Net	28.48	0.885	26.91	0.860	28.93	0.885	30.43	0.904	29.86	0.897
	TRG-Net	<b>28.58</b>	<b>0.888</b>	<b>27.01</b>	<b>0.862</b>	<b>29.00</b>	<b>0.886</b>	<b>30.52</b>	<b>0.905</b>	<b>30.27</b>	<b>0.906</b>

method, but also more superior for deraining and downstream tasks.

### 5.3 Rain Data Augmentation for Paired Data Set

In this section, we perform rain data augmentation, including in-distribution and out-of-distribution augmentation, for deraining on paired datasets. Specifically, we first conduct in-distribution rain augmentation for deraining on synthetic datasets (Sec. 5.3.1) and real SPA-Data (Sec. 5.3.2) to demonstrate the diversity of generated rain data. Then, OOD rain augmentation, including the orientation and sparsity of rain, are implemented in Sec. 5.3.3 to further validate the controllability superiority of TRG-Net.

#### 5.3.1 Rain Data Augmentation on Synthetic Datasets

**Datasets and deraining models.** Two commonly used synthetic rain datasets, Rain100L and Rain100H [7], are employed to evaluate the performance of data augmentation by rain generators for deraining. Rain100H is a large-scale dataset, which contains 1800 pairs of rainy and rainless images for training and 100 rainy/rainless images for testing. We also construct two relatively small datasets, Rain100L-S and Rain100H-S, where the training sets are the first 100 pairs of training

images from Rain100L and Rain100H, respectively, and the test sets from the test sets of Rain100L and Rain100H, respectively, to further evaluate the performance of data augmentation. We leverage five classical and SOTA deraining models, including PReNet [32], SPANet [25], JORDER\_E [27], RCDNet [39] and DRSformer [34], to evaluate the performance of the proposed generator compared to VRG-Net.

**Training details of the generator.** For a fair comparison with the current SOTA rain generator, VRG-Net [18], we exploit the same discriminator as VRG-Net, i.e., a self-attention discriminator [53] with gradient penalty. The batch size and patch size are set as 10 and  $128 \times 128$ , respectively. The rotatable TV regularizer is adopted for the training of Rain100L and Rain100L-S. The rain generator is trained for 200 epochs on Rain100L and Rain100L-S, and 400 epochs on Rain100H and Rain100H-S. The other training settings are those used in Sec. 5.1. The augmentation rate is set as 0.5 for Rain100L, Rain100L-S and Rain100H-S, and 1% for Rain100H. Note that we input paired clean background  $\mathcal{B}$  and rainy image  $\mathcal{X}$  for training the rainy image generators, which will lead to better performance than training the model with unpaired samples.

**Evaluation on synthetic data.** Table 4 provides the deraining results of all competing methods without and with data augmentation,



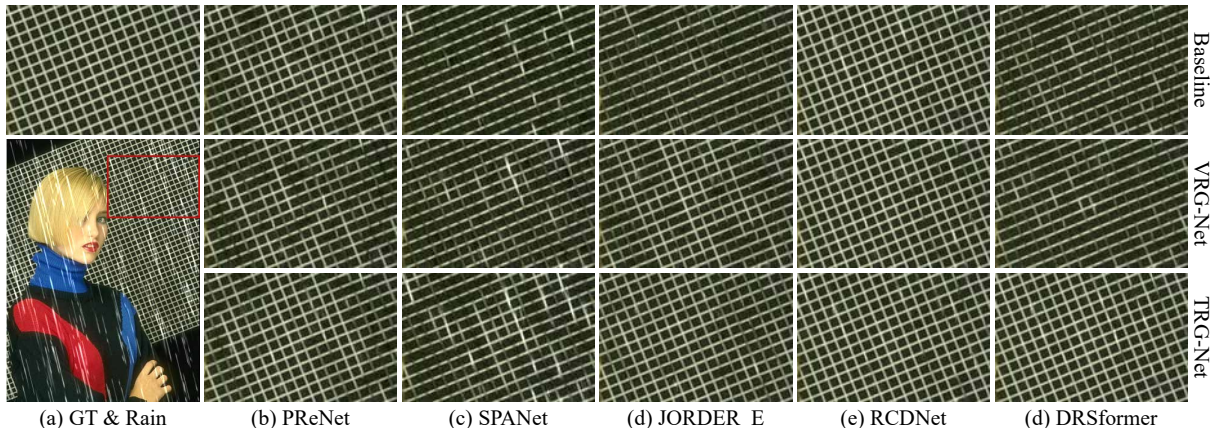


**Fig. 10** Comparison of deraining results on a test simple from Rain100L-S. (a): The rainy image and groundtruth on Rain100L-S test set. (b)-(e): From top to bottom: the deraining results trained on the original Rain100L-S, augmented data generated by VRG-Net, and augmented data generated by the proposed TRG-Net, respectively, where the deraining methods from left to right are PReNet, SPANet, JORDER\_E, RCDNet and DRSformer, respectively.

**Table 5** The generalization performance on SPA-Data. Baseline means the derainers trained on the original dataset without augmentation. VRG-Net and TRG-Net denote augmented training using VRG-Net and the proposed TRG-Net, respectively. The best result is highlighted with **bold**.

Datasets	Methods	PReNet		SPANet		JORDER_E		RCDNet		DRSformer	
		PSNR	SSIM	PSNR	SSIM	PSNR	SSIM	PSNR	SSIM	PSNR	SSIM
Rain100L	Baseline	34.95	0.941	35.18	0.946	35.02	0.942	34.88	0.938	34.48	0.947
	VRG-Net	34.97	0.943	35.43	0.946	35.10	0.942	34.84	0.939	<b>34.77</b>	0.949
	TRG-Net	<b>35.50</b>	<b>0.949</b>	<b>35.50</b>	<b>0.948</b>	<b>35.78</b>	<b>0.950</b>	<b>35.59</b>	<b>0.948</b>	<b>34.77</b>	<b>0.952</b>
Rain100L-S	Baseline	34.88	0.941	35.17	0.945	35.14	0.942	35.00	0.941	34.41	0.948
	VRG-Net	35.08	0.943	<b>35.36</b>	<b>0.947</b>	35.17	0.943	35.03	0.941	34.52	0.948
	TRG-Net	<b>35.24</b>	<b>0.947</b>	35.35	<b>0.947</b>	<b>35.65</b>	<b>0.949</b>	<b>35.53</b>	<b>0.949</b>	<b>34.96</b>	<b>0.952</b>
Rain100H	Baseline	33.10	0.934	32.72	0.942	33.59	0.941	34.25	<b>0.944</b>	34.25	0.945
	VRG-Net	33.99	<b>0.943</b>	32.77	0.942	34.76	<b>0.946</b>	33.70	<b>0.944</b>	34.47	0.945
	TRG-Net	<b>34.14</b>	<b>0.943</b>	<b>33.22</b>	<b>0.943</b>	<b>35.06</b>	<b>0.946</b>	<b>34.26</b>	<b>0.944</b>	<b>34.52</b>	<b>0.948</b>
Rain100H-S	Baseline	33.73	0.940	31.50	0.931	33.24	0.935	34.36	0.944	34.22	0.946
	VRG-Net	33.76	0.942	31.49	0.931	33.18	0.934	34.05	0.943	33.54	0.943
	TRG-Net	<b>34.24</b>	<b>0.943</b>	<b>31.85</b>	<b>0.933</b>	<b>33.49</b>	<b>0.939</b>	<b>34.52</b>	<b>0.945</b>	<b>34.24</b>	<b>0.948</b>

on four datasets. “Baseline” denotes the performance of the derainers trained on the original data set without data augmentation here. As shown in Table 4, the deraining performance of every deep derainer gains a significant improvement with data augmentation in most cases. The performance achieves more improvement on Rain100L-S and Rain100H-S, which accords with human intuition that data augmentation will have more effects when there are less training samples.

These results imply that the rainy images generated by the proposed TRG-Net should be closer to those of the original data, which leads to better performance compared to VRG-Net. Fig. 10 visualizes the deraining results of all competing methods on a typical image of Rain100L-S without and with data augmentation. We can observe that the results with TRG-Net augmentation not only more evidently remove rains, but also better preserve the texture and edges of the image.

**Table 6** The average PSNR and SSIM of PReNet on the SPA-Data test set. The training set of Baseline is all from original SPA-Data. The training data of VRG-Net and the proposed TRG-Net consist of real pairs randomly selected from SPA-Data and fake pairs generated by different generators. We report the mean of five repeated experiments. The best result is highlighted with **bold**.

#Real-samples	1K		1.5K		2K		3K		4K		~630K	
	PSNR	SSIM	PSNR	SSIM	PSNR	SSIM	PSNR	SSIM	PSNR	SSIM	PSNR	SSIM
Baseline	39.41	0.9787	39.70	0.9800	39.86	0.9809	39.96	0.9813	40.05	0.9815	40.68	0.9845
#Samples (real+fake)	1K+0K		1K+0.5K		1K+1K		1K+2K		1K+3K		2K+2K	
	PSNR	SSIM	PSNR	SSIM	PSNR	SSIM	PSNR	SSIM	PSNR	SSIM	PSNR	SSIM
VRG-Net[18]	39.41	0.9787	39.71	0.9796	39.83	0.9795	40.25	0.9813	40.24	0.9814	40.73	0.9830
TRG-Net	39.41	0.9787	<b>40.57</b>	<b>0.9826</b>	<b>41.18</b>	<b>0.9839</b>	<b>41.03</b>	<b>0.9834</b>	<b>41.09</b>	<b>0.9834</b>	<b>41.37</b>	<b>0.9850</b>

### Generalization evaluation on real data.

Table 5 shows the generalization performance of models trained on four synthetic datasets and tested on real rainy images of SPA-Data. In this case, the PSNR and SSIM with data augmentation by VRG-Net gain an unsubstantial advantage over the baseline in most cases. By comparison, the performance with data augmentation of TRG-Net still achieves a consistently obvious improvement over the baseline in most test cases. These results demonstrate that the samples generated by our method can improve the deraining performance not only in in-distribution but also in out-of-distribution tasks.

### 5.3.2 Rain Data Augmentation on Real SPA-Data

Following [18], we conduct rain data augmentation on SPA-Data [25], a real dataset containing over 630K pairs of rainy and rainless image patches for training and 1000 pairs of rainy and rainless images for testing, to further verify the diversity and comprehensiveness of the generated rains.

**Experiment settings.** The generator is trained for 400 epochs. The other training settings of TRG-Net are the same as those settings in Sec. 5.3.1. The rain generators are first trained on SPA-Data in a paired manner. Then we take PReNet [32] as the derainer. The training data for the derainer consist of a small number of pairs (i.e., 1K and 2K) randomly selected from SPA-Data and  $NK$  fake pairs generated by the generators. For comparison, the same number of paired data from SPA-Data is also randomly chosen as the training

set of the derainer, which is called “Baseline” in this experiment.

**The experimental results.** The PSNR and SSIM on the test set of SPA-Data are shown in Table 6<sup>8</sup>. From Table 6, we can observe that better performance can be achieved with generated data samples than that with even more original data samples<sup>9</sup>. In addition, the derainer trained on the samples generated by the proposed TRG-Net obtains a better result than those trained on the same and even more number of data samples generated by the VRG-Net [18]. These results validate the superior quality of the generated samples by the proposed TRG-Net beyond those generated by VRG-Net.

### 5.3.3 OOD Rain Augmentation

To further verify the superiority of our controllable rain generation, we generate OOD rain for OOD deraining by controlling the rain factors of trained TRG-Net. Specifically, the two main factors influencing the appearance of rain, namely orientation and sparsity, are augmented in the following.

**Rain orientation augmentation.** In this experiment, we synthesize 200 pairs of training images containing only  $-30^\circ$  to  $30^\circ$  degree orientation rains from rainless images of Rain100L, and construct two test sets with different orientation

<sup>8</sup>To avoid randomness of the experiment, we report the mean of five repetitive experiments following [18].

<sup>9</sup>This can be rationally explained by the fact that the generated rainy images are with much less repetitively but possibly with a more diversity (possibly even generating new rain patterns that not appear in the original training data, as the previous analysis) in a highly controllable manner than the original training data.



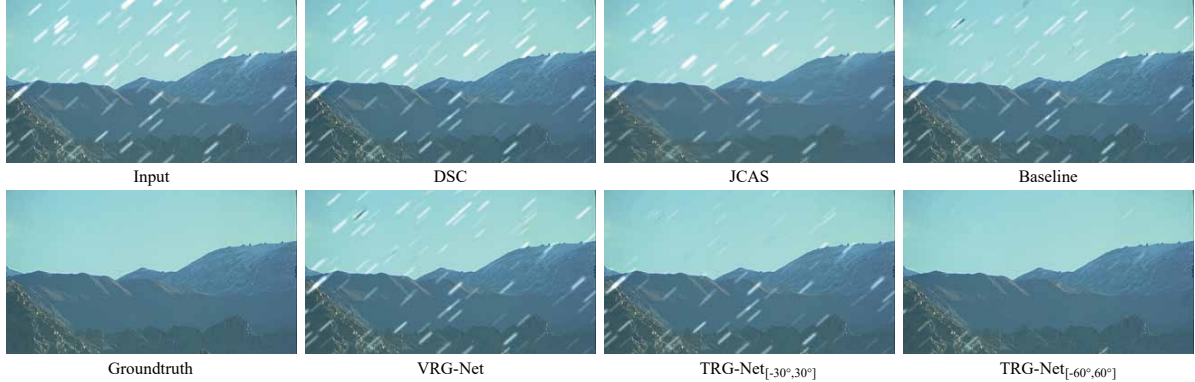


**Fig. 11** The visual deraining results of a typical image in the test rainy images with orientation degrees  $\pm[30^\circ, 60^\circ]$ . Upper row: from left to right are the input rainy image, deraining results of DSC [49], JCAS [50] and PReNet [32] without data augmentation, respectively. Lower row: from left to right are the groundtruth, deraining results of PReNet augmented on VRG-Net [18], TRG-Net $_{[-30^\circ, 30^\circ]}$ , TRG-Net $_{[-60^\circ, 60^\circ]}$ , respectively.

**Table 7** The PSNR and SSIM comparison on test data with orientation degree of  $[-30^\circ, 30^\circ]$  and  $\pm[30^\circ, 60^\circ]$ . Baseline represents the deraining results of PReNet [32] trained on original training set. VRG-Net, TRG-Net $_{[-30^\circ, 30^\circ]}$  and TRG-Net $_{[-60^\circ, 60^\circ]}$  are the deraining results of PReNet augmented on VRG-Net, TRG-Net $_{[-30^\circ, 30^\circ]}$  and TRG-Net $_{[-60^\circ, 60^\circ]}$ , respectively.

Methods	in-distribution		out-of-distribution	
	[-30°, 30°]		±[30°, 60°]	
	PSNR	SSIM	PSNR	SSIM
Input	23.23	0.846	23.52	0.853
DSC [49]	24.98	0.861	24.00	0.848
JCAS [50]	25.24	0.867	24.72	0.852
Baseline	37.92	0.985	26.58	0.885
VRG-Net [18]	38.33	<b>0.986</b>	26.52	0.886
TRG-Net $_{[-30^\circ, 30^\circ]}$	<b>38.58</b>	<b>0.986</b>	27.59	0.899
TRG-Net $_{[-60^\circ, 60^\circ]}$	38.44	<b>0.986</b>	<b>29.06</b>	<b>0.926</b>

degree ranges of rains. One test set contains rains with orientation degrees from  $-30^\circ$  to  $30^\circ$ , named as  $[-30^\circ, 30^\circ]$ , and the other contains rains with degrees from  $-60^\circ$  to  $-30^\circ$  and  $30^\circ$  to  $60^\circ$ , called  $\pm[30^\circ, 60^\circ]$ . In the training phase for deraining networks, we augment the training data with the same orientation as the training set using generators (i.e. VRG-Net and TRG-Net $_{[-30^\circ, 30^\circ]}$  in Table 7). While for TRG-Net, due to its rain factor controllability, one can augment the training data into a wider range of orientation degrees. Specifically, we augment the orientation degrees of the rains from  $-60^\circ$  to  $60^\circ$  by the proposed TRG-Net, and denote the result as TRG-Net $_{[-60^\circ, 60^\circ]}$ . The experimental results are shown in Table 7, where “Baseline” indicates the deraining result of PReNet trained on original training set. We

also list the deraining results of two model-based methods, DSC [49] and JCAS [50]. We can see that Baseline and VRG-Net achieve a relatively poor performance when the orientation of the rain distribution in the test set differs from the training set. Comparatively, the proposed methods not only perform better on test data with orientation range in  $[-30^\circ, 30^\circ]$ , but also have a well performance on rain orientation range in  $\pm[30^\circ, 60^\circ]$ . Specifically, the augmented training on TRG-Net $_{[-60^\circ, 60^\circ]}$  achieves a significant performance improvement in  $\pm[30^\circ, 60^\circ]$  case. Fig. 11 depicts the visual deraining result on  $\pm[30^\circ, 60^\circ]$  and we can observe that only TRG-Net $_{[-60^\circ, 60^\circ]}$  removes the rain streaks effectively.

**Rain sparsity augmentation.** We select the 50mm/hr rain data from the training set of Cityscapes [30] as our training set. The test rain datasets are collected from the test sets of Cityscapes, incorporating different rainfall rates, ranging from 5mm/hr to 100mm/hr. Firstly, the rain generators are trained on 50mm/hr training set. Then, in the training phase for deraining, we use PReNet trained on original 50mm/hr training set as the baseline and further augment the training data through in-distribution augmentation using VRG-Net and TRG-Net. While for TRG-Net, out-of-distribution sparsity rain data are augmented by controlling the sparsity factor of TRG-Net, which is indicated as TRG-Net $^\dagger$ . The deraining performance of all competing methods on all test sets are shown in Table 8. The performance of deraining on out-of-distribution

**Table 8** The deraining performance on Cityscapes with varying levels of sparsity. Baseline represents the deraining results of PReNet trained on original training set. VRG-Net, TRG-Net are the deraining results of PReNet through in-distribution augmentation on VRG-Net and TRG-Net, respectively. TRG-Net<sup>†</sup> denotes the deraining results of augmented PReNet on out-of-distribution rain by controlling the sparsity using TRG-Net. The best result is highlighted with **bold**.

Methods	out-of-distribution				in-distribution		out-of-distribution			
	5mm/hr		25mm/hr		50mm/hr		75mm/hr		100mm/hr	
	PSNR	SSIM	PSNR	SSIM	PSNR	SSIM	PSNR	SSIM	PSNR	SSIM
Baseline	34.20	<b>0.995</b>	28.70	<b>0.990</b>	23.58	0.976	21.42	0.963	20.21	0.952
VRG-Net[18]	33.24	<b>0.995</b>	28.20	<b>0.990</b>	23.58	0.976	21.35	0.962	20.10	0.950
TRG-Net	34.33	<b>0.995</b>	29.00	<b>0.990</b>	<b>24.75</b>	<b>0.979</b>	21.88	0.964	20.48	0.952
TRG-Net <sup>†</sup>	<b>34.53</b>	<b>0.995</b>	<b>29.15</b>	<b>0.990</b>	24.71	<b>0.979</b>	<b>22.00</b>	<b>0.966</b>	<b>20.58</b>	<b>0.954</b>

**Table 9** The FID and KID of generating rain by TRG-Net under different ablation settings.

Factor learning	MerNet	RotTV	FID	KID
×	✓	✓	42.93	0.0131
✓	×	✓	32.65	0.0090
✓	✓	×	29.69	0.0073
✓	✓	✓	<b>25.78</b>	<b>0.0047</b>

**Table 10** The deraining results of PReNet[32] trained on the pseudo-paired data generated by TRG-Net under different ablation settings.

Factor learning	MerNet	RotTV	PSNR	SSIM
×	✓	✓	28.55	0.874
✓	×	✓	29.82	0.905
✓	✓	×	31.94	0.946
✓	✓	✓	<b>32.33</b>	<b>0.949</b>

sparsity rain is improved by implementing OOD rain sparsity augmentation.

## 5.4 Ablation Study

We conduct various ablation settings for the proposed TRG-Net. Firstly, we consider the effectiveness of the rain factor learning. Specifically, we replace transformable convolution kernels with common convolution kernels in our model, which is then degenerated to a CSC-based rain model without any rain factor input. Then we also consider the influence of the merging model and the proposed rotTV regularizer. All ablation experiments are performed on Rain100L in an unpaired way. Table 9 shows the FID and KID of generating rain by TRG-Net under different ablation settings. We can observe that the factor learning, merging model and rotTV all have effects

on the rain generation performance. In particular, Table 10 further shows the deraining performance of PReNet trained on the pseudo pairs generated by these different settings. It can be observed that all the aforementioned settings make a positive contribution to the deraining performance of the entire TRG-Net model, and the completeness of them achieves the best deraining performance.

## 6 Conclusion

In this paper, we have constructed a transformable rainy image generation network (TRG-Net), which intrinsically encodes the rain factors, including shape, orientation, length, width and sparsity, into the design of network and can properly extract these fundamental rain factors underlying rainy images purely from data. To the best our knowledge, TRG-Net should be the first rain generator that can not only elaborately design fundamental elements to simulate expected rains, like conventional artificial rendering methods, but also finely adapt to complicated and diverse practical rain patterns, like recent deep learning methods. A transformable convolution framework has been proposed to alleviate the difficulty in embedding controllable and learnable rain factors into deep networks. We have further presented a rotatable TV regularizer for rain generation, which is able to adaptively adjust the orientation for calculating variations and adopt higher penalty along the rain streak orientation. Comprehensive experiments on synthetic and real datasets have validated the superiority of the proposed TRG-Net beyond current SOTA rain generation methods in both unpaired rain generation and paired rain augmentation tasks.

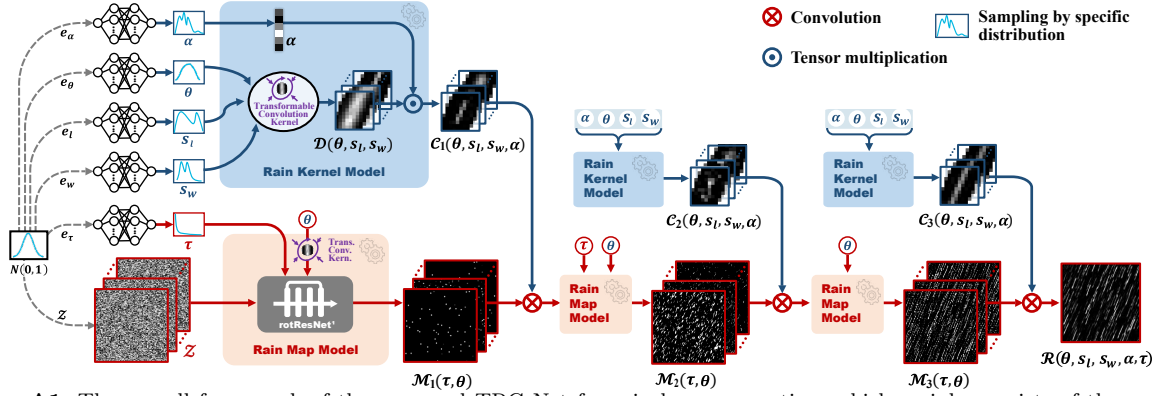


**Fig. A1** The overall framework of the proposed TRG-Net for rain layer generation, which mainly consists of three rain kernel models and three rain map models.

Although a reasonable rainy image generator has been proposed, we find empirically that the discriminator can have an impact on the performance of rain generation. Therefore, the design of the discriminator is also critical for stabilising the training of GAN. Besides, the proposed transformable convolution framework and the rotatable TV regularizer could have potential application value for extensive tasks, such as the design of the deraining network. We will try these designs in our future research.

## Appendix A More Details on The Proposed TRG-Net

Our experiments empirically show that a single layer convolution of the rain kernels with the rain maps is usually not sufficient to generate the diverse, complex and long rain streaks, therefore we actually generate three rain kernels and convolute them with the rain maps to increase the receptive field of rain kernel. The overall architecture of the proposed rain layer generation network is shown in Fig. A1. Specifically, the rain kernels in three convolutions share the same shape, orientation, length and width factors. For  $i = 1, 2, 3$ ,

$$C_i = \text{KerNet}_{w^{c_i}}(e_\theta, e_l, e_w, e_\alpha), \quad (\text{A1})$$

where  $\text{KerNet}(\cdot)$  is defined in the main text Eq. (15).  $w^{c_i} = \{w^{d_i}, w^\theta, w^l, w^w, w^\alpha\}$  represent all the to-be-learned parameters and  $\{e_\theta, e_l, e_w, e_\alpha\} \sim N(0, 1)$ . We can see that the parameters of rain factors ( $w^\theta, w^l, w^w, w^\alpha$ ) are shared, while the

parameter of rain kernel dictionary  $w^{d_i}$  is not shared. This ensures that the rain factors implied in rain datasets are shared with all rain kernels.

The rain maps in three convolutions are all generated by rotResNet and the sparsity factor  $\tau$  is encoded into first two rain map models. From Eq. (17) in the main text,

$$\mathcal{M}_1 = \text{ReLU}(\text{rotResNet}_{w^{r_1}}^1(\mathcal{Z}, \theta) - \tau), \quad (\text{A2})$$

where  $\mathcal{Z} \sim N(0, 1)$  is the input Gaussian noise and  $\text{rotResNet}^1$  is a rotatable ResNet with parameters  $w^{r_1}$ .  $\theta, \tau$  are the rain orientation and sparsity, respectively, which are defined in the main text Eqs. (13) and (18), respectively. The convolution output of the rain kernel  $C_1$  and the rain map  $\mathcal{M}_1$  is then fed into the rain map model to generate the rain map  $\mathcal{M}_2$ . That is

$$\mathcal{M}_2 = \text{ReLU}(\text{rotResNet}_{w^{r_2}}^2(C_1 \otimes \mathcal{M}_1, \theta) - \tau), \quad (\text{A3})$$

where  $\theta, \tau$  are shared with Eq. (A2). Similarly, the rain map model takes the convolution output of the rain kernel  $C_2$  and the rain map  $\mathcal{M}_2$  as input and outputs the final rain map. That is

$$\mathcal{M}_3 = \text{rotResNet}_{w^{r_3}}^3(C_2 \otimes \mathcal{M}_2, \theta), \quad (\text{A4})$$

where  $\theta$  is the orientation degree, which is shared with Eqs. (A2) and (A3).

Based on the proposed rain model (10) in the main text, the rain layer is generated by

$$\mathcal{R}(\tau, \theta, s_l, s_w) = C_3(\theta, s_l, s_w) \otimes \mathcal{M}_3(\tau, \theta), \quad (\text{A5})$$

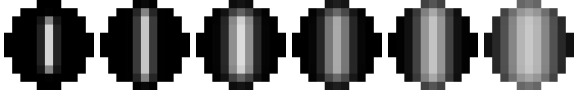


**Fig. A2** Some initialized rain kernel dictionaries to better understand the design of Eq. (A6).

where  $\mathcal{C}_3(\theta, s_l, s_w)$  is the third rain kernel generated by the rain kernel model, and  $\mathcal{M}_3(\tau)$  is the third rain map.

It should be noted that the rain kernel dictionary has an evident physical meaning, which is different from other convolution filters in deep networks. Therefore, we specifically design an initialization manner for it according to the prior knowledge of rains. Formally, the initialized rain kernel dictionary is sampled from

$$\tilde{\phi}(x) = A \cdot \exp\left(-25\sigma \|\text{ReLu}(|x| - w)\|_2^2\right) \quad (\text{A6})$$

where  $|x| = \begin{bmatrix} |x_1| \\ |x_2| \end{bmatrix}$ ,  $w = \begin{bmatrix} w_1 \\ w_2 \end{bmatrix}$ ,  $w_1 \sim N(0.001, 0.01)$ ,  $w_2 \sim N(0.5, 0.2)$ ,  $\sigma \sim N(0.1, 2)$ ,  $A \sim N(0.6, 0.3)$ . Fig. A2 shows some initialized rain kernel dictionaries for visual understanding of this design. Then, the initialization values of the parameter  $w^d$  in Eq. (12) of the main text can be easily obtained by adopting discrete Fourier transform on the initialized dictionary.

## Data Availability Statement

The data supporting the results of this study are available from the authors on request.

## Statements and Declarations

The authors declare that they have no known competing financial interests or personal relationships that could appear to have influenced the work reported in this paper.

## References

- [1] Wang, H., Wu, Y., Li, M., Zhao, Q., Meng, D.: Survey on rain removal from videos or a single image. *Science China Information Sciences* **65**(1), 1–23 (2022)
- [2] Yang, W., Tan, R.T., Wang, S., Fang, Y., Liu, J.: Single image deraining: From model-based to data-driven and beyond. *IEEE Transactions on pattern analysis and machine intelligence* **43**(11), 4059–4077 (2020)
- [3] Li, S., Araujo, I.B., Ren, W., Wang, Z., Tokuda, E.K., Junior, R.H., Cesar-Junior, R., Zhang, J., Guo, X., Cao, X.: Single image deraining: A comprehensive benchmark analysis. In: *Proceedings of the IEEE/CVF Conference on Computer Vision and Pattern Recognition*, pp. 3838–3847 (2019)
- [4] Wang, H., Xie, Q., Wu, Y., Zhao, Q., Meng, D.: Single image rain streaks removal: a review and an exploration. *International Journal of Machine Learning and Cybernetics* **11**(4), 853–872 (2020)
- [5] Bossu, J., Hautière, N., Tarel, J.-P.: Rain or snow detection in image sequences through use of a histogram of orientation of streaks. *International Journal of Computer Vision* **93**(3), 348–367 (2011) <https://doi.org/10.1007/s11263-011-0421-7>
- [6] Fu, X., Huang, J., Zeng, D., Huang, Y., Ding, X., Paisley, J.: Removing rain from single images via a deep detail network. In: *Proceedings of the IEEE Conference on Computer Vision and Pattern Recognition*, pp. 3855–3863 (2017)
- [7] Yang, W., Tan, R.T., Feng, J., Liu, J., Guo, Z., Yan, S.: Deep joint rain detection and removal from a single image. In: *Proceedings of the IEEE Conference on Computer Vision and Pattern Recognition*, pp. 1357–1366 (2017)
- [8] Garg, K., Nayar, S.K.: Photorealistic rendering of rain streaks. *ACM Transactions on Graphics (TOG)* **25**(3), 996–1002 (2006)
- [9] Garg, K., Nayar, S.K.: Vision and rain. *International Journal of Computer Vision* **75**(1), 3–27 (2007)
- [10] Weber, Y., Jolivet, V., Gilet, G., Ghazanfarpour, D.: A multiscale model for rain rendering in real-time. *Computers & Graphics* **50**, 61–70 (2015)

- [11] Starik, S., Werman, M.: Simulation of rain in videos. In: Texture Workshop, ICCV, vol. 2, pp. 406–409 (2003)
- [12] Wang, L., Lin, Z., Fang, T., Yang, X., Yu, X., Kang, S.B.: Real-time rendering of realistic rain. In: ACM SIGGRAPH 2006 Sketches, p. 156 (2006)
- [13] Wei, W., Meng, D., Zhao, Q., Xu, Z., Wu, Y.: Semi-supervised transfer learning for image rain removal. In: Proceedings of the IEEE/CVF Conference on Computer Vision and Pattern Recognition, pp. 3877–3886 (2019)
- [14] Yasarla, R., Sindagi, V.A., Patel, V.M.: Syn2real transfer learning for image deraining using gaussian processes. In: Proceedings of the IEEE/CVF Conference on Computer Vision and Pattern Recognition, pp. 2726–2736 (2020)
- [15] Goodfellow, I., Pouget-Abadie, J., Mirza, M., Xu, B., Warde-Farley, D., Ozair, S., Courville, A., Bengio, Y.: Generative adversarial nets. *Advances in neural information processing systems* **27** (2014)
- [16] Zhu, J.-Y., Park, T., Isola, P., Efros, A.A.: Unpaired image-to-image translation using cycle-consistent adversarial networks. In: Proceedings of the IEEE International Conference on Computer Vision, pp. 2223–2232 (2017)
- [17] Isola, P., Zhu, J.-Y., Zhou, T., Efros, A.A.: Image-to-image translation with conditional adversarial networks. In: Proceedings of the IEEE Conference on Computer Vision and Pattern Recognition, pp. 1125–1134 (2017)
- [18] Wang, H., Yue, Z., Xie, Q., Zhao, Q., Zheng, Y., Meng, D.: From rain generation to rain removal. In: Proceedings of the IEEE/CVF Conference on Computer Vision and Pattern Recognition, pp. 14791–14801 (2021)
- [19] Choi, J., Kim, D.H., Lee, S., Lee, S.H., Song, B.C.: Synthesized rain images for deraining algorithms. *Neurocomputing* **492**, 421–439 (2022)
- [20] Ni, S., Cao, X., Yue, T., Hu, X.: Controlling the rain: From removal to rendering. In: Proceedings of the IEEE/CVF Conference on Computer Vision and Pattern Recognition, pp. 6328–6337 (2021)
- [21] Wei, Y., Zhang, Z., Wang, Y., Xu, M., Yang, Y., Yan, S., Wang, M.: Deraincyclegan: Rain attentive cyclegan for single image deraining and rainmaking. *IEEE Transactions on Image Processing* **30**, 4788–4801 (2021)
- [22] Chen, X., Pan, J., Jiang, K., Li, Y., Huang, Y., Kong, C., Dai, L., Fan, Z.: Unpaired deep image deraining using dual contrastive learning. In: 2022 IEEE/CVF Conference on Computer Vision and Pattern Recognition (CVPR), pp. 2007–2016. IEEE, ??? (2022)
- [23] Hu, X., Fu, C.-W., Zhu, L., Heng, P.-A.: Depth-attentional features for single-image rain removal. In: Proceedings of the IEEE/CVF Conference on Computer Vision and Pattern Recognition, pp. 8022–8031 (2019)
- [24] Xie, Q., Zhao, Q., Xu, Z., Meng, D.: Fourier series expansion based filter parametrization for equivariant convolutions. *IEEE Transactions on Pattern Analysis and Machine Intelligence* (2022)
- [25] Wang, T., Yang, X., Xu, K., Chen, S., Zhang, Q., Lau, R.W.: Spatial attentive single-image deraining with a high quality real rain dataset. In: Proceedings of the IEEE/CVF Conference on Computer Vision and Pattern Recognition, pp. 12270–12279 (2019)
- [26] Li, W., Zhang, Q., Zhang, J., Huang, Z., Tian, X., Tao, D.: Toward real-world single image deraining: A new benchmark and beyond. *arXiv preprint arXiv:2206.05514* (2022)
- [27] Yang, W., Tan, R.T., Feng, J., Guo, Z., Yan, S., Liu, J.: Joint rain detection and removal from a single image with contextualized deep networks. *IEEE transactions on pattern analysis and machine intelligence* **42**(6), 1377–1393 (2019)



- [28] Zhang, H., Sindagi, V., Patel, V.M.: Image de-raining using a conditional generative adversarial network. *IEEE transactions on circuits and systems for video technology* **30**(11), 3943–3956 (2019)
- [29] Halder, S.S., Lalonde, J.-F., Charette, R.d.: Physics-based rendering for improving robustness to rain. In: *Proceedings of the IEEE/CVF International Conference on Computer Vision*, pp. 10203–10212 (2019)
- [30] Tremblay, M., Halder, S.S., De Charette, R., Lalonde, J.-F.: Rain rendering for evaluating and improving robustness to bad weather. *International Journal of Computer Vision* **129**(2), 341–360 (2021)
- [31] Pizzati, F., Cerri, P., Charette, R.d.: Model-based occlusion disentanglement for image-to-image translation. In: *European Conference on Computer Vision*, pp. 447–463 (2020). Springer
- [32] Ren, D., Zuo, W., Hu, Q., Zhu, P., Meng, D.: Progressive image deraining networks: A better and simpler baseline. In: *Proceedings of the IEEE/CVF Conference on Computer Vision and Pattern Recognition*, pp. 3937–3946 (2019)
- [33] Wang, H., Xie, Q., Zhao, Q., Liang, Y., Meng, D.: Rcdnet: An interpretable rain convolutional dictionary network for single image deraining. *arXiv preprint arXiv:2107.06808* (2021)
- [34] Chen, X., Li, H., Li, M., Pan, J.: Learning a sparse transformer network for effective image deraining. In: *Proceedings of the IEEE/CVF Conference on Computer Vision and Pattern Recognition*, pp. 5896–5905 (2023)
- [35] Ye, Y., Yu, C., Chang, Y., Zhu, L., Zhao, X.-L., Yan, L., Tian, Y.: Unsupervised deraining: Where contrastive learning meets self-similarity. In: *Proceedings of the IEEE/CVF Conference on Computer Vision and Pattern Recognition*, pp. 5821–5830 (2022)
- [36] Weiler, M., Hamprecht, F.A., Storath, M.: Learning steerable filters for rotation equivariant cnns. In: *Proceedings of the IEEE Conference on Computer Vision and Pattern Recognition*, pp. 849–858 (2018)
- [37] Weiler, M., Cesa, G.: General e (2)-equivariant steerable cnns. *Advances in Neural Information Processing Systems* **32** (2019)
- [38] Li, M., Xie, Q., Zhao, Q., Wei, W., Gu, S., Tao, J., Meng, D.: Video rain streak removal by multiscale convolutional sparse coding. In: *Proceedings of the IEEE Conference on Computer Vision and Pattern Recognition*, pp. 6644–6653 (2018)
- [39] Wang, H., Xie, Q., Zhao, Q., Meng, D.: A model-driven deep neural network for single image rain removal. In: *Proceedings of the IEEE/CVF Conference on Computer Vision and Pattern Recognition*, pp. 3103–3112 (2020)
- [40] He, K., Zhang, X., Ren, S., Sun, J.: Deep residual learning for image recognition. In: *Proceedings of the IEEE Conference on Computer Vision and Pattern Recognition*, pp. 770–778 (2016)
- [41] Nair, V., Hinton, G.E.: Rectified linear units improve restricted boltzmann machines. In: *Proceedings of the 27th International Conference on Machine Learning (ICML-10)*, pp. 807–814 (2010)
- [42] Rudin, L.I., Osher, S., Fatemi, E.: Nonlinear total variation based noise removal algorithms. *Physica D* **60**(1-4), 259–268 (1992)
- [43] Mahendran, A., Vedaldi, A.: Understanding deep image representations by inverting them. In: *Proceedings of the IEEE Conference on Computer Vision and Pattern Recognition*, pp. 5188–5196 (2015)
- [44] Liu, Y., Yue, Z., Pan, J., Su, Z.: Unpaired learning for deep image deraining with rain direction regularizer. In: *Proceedings of the IEEE/CVF International Conference on Computer Vision*, pp. 4753–4761 (2021)

- [45] Zhuang, J.-H., Luo, Y.-S., Zhao, X.-L., Jiang, T.-X.: Reconciling hand-crafted and self-supervised deep priors for video directional rain streaks removal. *IEEE Signal Processing Letters* **28**, 2147–2151 (2021)
- [46] Zhuang, J., Luo, Y., Zhao, X., Jiang, T., Guo, B.: Uconnet: Unsupervised controllable network for image and video deraining. In: *Proceedings of the 30th ACM International Conference on Multimedia*, pp. 5436–5445 (2022)
- [47] Gulrajani, I., Ahmed, F., Arjovsky, M., Dumoulin, V., Courville, A.C.: Improved training of wasserstein gans. *Advances in neural information processing systems* **30** (2017)
- [48] Kingma, D.P., Ba, J.: Adam: A method for stochastic optimization. *arXiv preprint arXiv:1412.6980* (2014)
- [49] Luo, Y., Xu, Y., Ji, H.: Removing rain from a single image via discriminative sparse coding. In: *Proceedings of the IEEE International Conference on Computer Vision*, pp. 3397–3405 (2015)
- [50] Gu, S., Meng, D., Zuo, W., Zhang, L.: Joint convolutional analysis and synthesis sparse representation for single image layer separation. In: *Proceedings of the IEEE International Conference on Computer Vision*, pp. 1708–1716 (2017)
- [51] Romera, E., Alvarez, J.M., Bergasa, L.M., Arroyo, R.: Erfnet: Efficient residual factorized convnet for real-time semantic segmentation. *IEEE Transactions on Intelligent Transportation Systems* **19**(1), 263–272 (2017)
- [52] Li, R., Cheong, L.-F., Tan, R.T.: Heavy rain image restoration: Integrating physics model and conditional adversarial learning. In: *Proceedings of the IEEE/CVF Conference on Computer Vision and Pattern Recognition*, pp. 1633–1642 (2019)
- [53] Zhang, H., Goodfellow, I., Metaxas, D., Odena, A.: Self-attention generative adversarial networks. In: *International Conference on Machine Learning*, pp. 7354–7363 (2019).